

Colloquium: Structural, electronic and transport properties of silicon nanowires

Riccardo Rurali*

*Departament d'Enginyeria Electrònica, Universitat Autònoma de Barcelona,
08193 Bellaterra, Spain and
Institut de Ciència de Materials de Barcelona (CSIC), Campus de Bellaterra,
08193 Bellaterra, Barcelona, Spain*

(Dated: September 19, 2018)

Abstract

In this paper we review the theory of silicon nanowires. We focus on nanowires with diameters below 10 nm, where quantum effects become important and the properties diverge significantly from those of bulk silicon. These wires can be efficiently treated within electronic structure simulation methods and will be among the most important functional blocks of future nanoelectronic devices. Firstly, we review the structural properties of silicon nanowires, emphasizing the close connection between the growth orientation, the cross-section and the bounding facets. Secondly, we discuss the electronic structure of pristine and doped nanowires, which hold the ultimate key for their applicability in novel electronic devices. Finally, we review transport properties where some of the most important limitations in the performances of nanowire-based devices can lay. Many of the unique properties of these systems are at the same time defying challenges and opportunities for great technological advances.

*Electronic address: rrurali@icmab.es

Contents

I. Introduction	3
II. Structural properties	6
A. Growth orientations and monocrystallinity	6
B. Surface reconstructions in pristine nanowires	7
C. Passivated nanowires	9
D. Mechanical properties of nanowires	12
III. Electronic properties	14
A. Pristine Nanowires	14
B. Passivated nanowires	16
1. Band structure and band gap anisotropy	16
2. Quantum confinement	19
3. Surface chemistry	22
C. Doped and defective nanowires	24
1. Surface segregation, surface traps and dopant aggregation	24
2. Quantum confinement	27
3. Dielectric confinement	28
4. Metallic impurities	29
5. Formation energy	30
IV. Transport properties	32
A. Electron transport	32
1. Surface roughness disorder	32
2. Single-impurity scattering	33
3. Multiple-impurity scattering	34
4. Charged impurity scattering	35
B. Heat transport	36
V. Conclusions	39
Acknowledgments	40

I. INTRODUCTION

One-dimensional nanostructured systems have attracted a great attention in the last two decades, with this interest extraordinary boosted by the facile synthesis of carbon nanotubes (CNTs) reported in the beginning of the 90s (Iijima, 1991). The reason is twofold: on the one hand they have proved to be an excellent test-bed to study the most intriguing physical effects, whereas on the other hand they are believed to be among the most important building blocks of the next generation of electronic devices.

CNTs are hollow cylinders obtained by rolling up one or more graphene sheets, a one-atom-thick allotrope of carbon (Charlier *et al.*, 2007). The symmetry and the electronic structure of graphene (Neto *et al.*, 2009) are such that the properties of the CNT depends critically on the *exact* way it is wrapped up, and it can be either metallic or semiconducting. This confer the CNTs with a richer physics, but it is clearly far from ideal from the viewpoint of applications, especially when –as it is the case– a simple route to selectively grow one type of CNT or the other is lacking.

Nanowires are an extremely attractive alternative to CNTs, because it is much easier to control their electrical properties and, as long as the surface is properly passivated –something that occurs naturally during or right after growth–, they are invariably semiconducting ¹.

Silicon nanowires (SiNWs), in particular, look like a very appealing choice, since they provide the ideal interface with the existing Si devices, while taking advantage from a tractable material technology. SiNWs are commonly grown by the vapor-liquid-solid technique (Wagner and Ellis, 1964; Westwater *et al.*, 1997), where a Au nanoparticle is used to catalyze SiH₄ decomposition. Briefly, the Au particle is deposited onto a Si surface and react with the Si atoms of the substrate, forming Au-Si alloy droplets. These droplets adsorb Si

¹ Below we will discuss explicitly a few cases where nanowires derived from semiconducting solids can be metallic, whereas nanowires made of metal atoms are beyond the scope of this paper and are not being discussed.

from the vapor phase, resulting in a supersaturated state where the Si atoms precipitate and the SiNW starts nucleating ².

As David K. Ferry illustrates in an enlightening paper (Ferry, 2008), nanowires could provide the paradigm shift needed to continue improving the density and the performances of electronic circuits. For almost four decades the increase in computing power has been described by the well-known Moore's law (Moore, 1965), which has been standing on three pillars: (a) the increase of the size of the microchips; (b) the reduction of the transistor size, and (c) the *circuit cleverness*, that is the reduction of the number of devices required to perform a certain function. While the first of these driving forces played a significant role only in the pioneering years of solid state electronics, the reduction of device size has a pivotal role, since the physical limit of material scaling is rapidly approaching. Nanowires can lead to an obvious benefit concerning the miniaturization, thanks to bottom-up growth that allows overcoming the limit of conventional lithography-based top-down design. Subtler are the perspective advantages concerning circuit cleverness, which can be significantly improved by taking advantage of the coexisting nature of interconnection and active device of nanowires. In particular, a replacement of metallic *vias* with vertical transistors is envisaged. These new circuits could be easily reconfigured to perform different operations, achieving a much higher level of integration (Ferry, 2008). Additionally, compared to classical planar device technology, nanowires can better accommodate *all-around* gates (see Fig. 1), which improve field-effect efficiency and device performances (Colinge, 2004; Ng *et al.*, 2004) and mobilities of $\sim 1000 \text{ cm}^2\text{V}^{-1}\text{s}^{-1}$, substantially larger than those obtained in conventional Si devices, have been obtained (Cui *et al.*, 2003) ³.

Several promising applications have already been demonstrated, ranging from electron devices (Chung *et al.*, 2000; Cui and Lieber, 2001; Cui *et al.*, 2003; Goldberger *et al.*, 2006; Hu *et al.*, 2008; Lu *et al.*, 2008b; Wang *et al.*, 2006b; Yu *et al.*, 2000; Zheng *et al.*, 2004), logic gates (Huang *et al.*, 2001), non-volatile memories (Duan *et al.*, 2002), photovoltaics (Kempa *et al.*, 2008; Tian *et al.*, 2009, 2007), photonics (Gudiksen *et al.*, 2002;

² See Wang *et al.* (2008) for a comprehensive review of the growth techniques.

³ It is difficult to make rigorous comparisons, because the mobility has a strong inverse dependence on the dopant density which is seldom known with accuracy in nanowires. However, the peak value of $1350 \text{ cm}^2\text{V}^{-1}\text{s}^{-1}$ obtained for the hole mobility by Cui *et al.* (2003) must be compared with the typical values for bulk Si of $\sim 400 \text{ cm}^2\text{V}^{-1}\text{s}^{-1}$ and $\sim 100 \text{ cm}^2\text{V}^{-1}\text{s}^{-1}$ for an acceptor concentration of 10^{16} cm^{-3} and 10^{18} cm^{-3} , respectively.

Pauzauskie and Yang, 2006), to biological sensors (Cui *et al.*, 2001b; Hahm and Lieber, 2004; Zhong *et al.*, 2003). On top of that, giant piezoresistance effect (He and Yang, 2006) and enhanced thermoelectric performances (Boukai *et al.*, 2008; Hochbaum *et al.*, 2008) have recently been reported. The interested reader is encouraged to check some of the many experimental reviews (Kumar, 2007; Li *et al.*, 2006; Lu and Lieber, 2006; Patolsky and Lieber, 2005; Thelander *et al.*, 2006; Wu *et al.*, 2008a; Xia *et al.*, 2003).

In this paper we will review the theory of SiNWs. Clearly, we will make several references to experiments, whenever they support or challenge the theoretical predictions. Sometimes the comparisons are difficult to make, because SiNWs that are routinely grown range from 50 to 200 nm, while those that can be efficiently studied within electronic structure methods are 2-3 nm thick, at most. Luckily, this gap is slowly narrowing and thin SiNWs with diameters below 10 nm have been successfully grown by several groups (Coleman *et al.*, 2001a,b; Cui *et al.*, 2001a, 2003; De Padova *et al.*, 2008; Holmes *et al.*, 2000; Ma *et al.*, 2003; Morales and Lieber, 1998; Wu *et al.*, 2004; Zhong *et al.*, 2005). The theoretical results that we discuss outline the most urgent problems that will have to be dealt with within the next generation of nanowires, those with characteristic sizes approaching the quantum limit.

Although many of the features that we will discuss are common to other types of semiconducting nanowires, for the sake of clarity we will restrict to SiNWs throughout the paper. It should be at least pointed out, however, that in recent years tremendous progresses are being made with compound semiconductors nanowires –mainly III-V nanowires– especially for what concerns photonics application (Björk *et al.*, 2002; Dick *et al.*, 2004; Thelander *et al.*, 2003).

A final remark concerns the computational methodologies. Although the main goal of the paper is giving a complete overview of the most important results that have been obtained within atomistic simulations, we will not enter in technical details, unless where it is necessary. Most of the results have been obtained within density functional theory (DFT), whose theoretical grounds are clearly out of the scope of this work. The interested reader can look at both the original papers (Hohenberg and Kohn, 1964; Kohn and Sham, 1965), excellent reviews (Jones and Gunnarsson, 1989; Payne *et al.*, 1992) and comprehensive books (Martin, 2004). Less frequently, we will refer to the tight-binding formalism (Colombo, 2005; Goringe *et al.*, 1997; Slater and Koster, 1954) or to empirical interatomic potentials (Justo *et al.*, 1998; Stillinger and Weber, 1985; Tersoff, 1989).

II. STRUCTURAL PROPERTIES

A. Growth orientations and monocrystallinity

The extraordinary impact that the discovery of carbon nanotubes (Iijima, 1991; Oberlin *et al.*, 1976; Radushkevich and Lukyanovich, 1952) had on condensed matter and nanoscience at first biased the research on Si quasi one-dimensional systems to the pursuit of tubular structures. Hollow structures resembling carbon nanotubes (Li *et al.*, 2002), structures based on hollow elements (Menon and Richter, 1999) or on fullerene-like system (Marsen and Sattler, 1999) have been proposed. Although these –or other structures inspired by cluster assemble (Sen *et al.*, 2002)– are stable within a total energy framework, they have not been observed experimentally to date.

In the meanwhile Si nanotubes have been indeed successfully synthesized (Sha *et al.*, 2002), while their use for nanoelectronics still remains troublesome (Perepichka and Rosei, 2006), and things with Si nanowires turned out to be simpler than speculated. Convincing experimental evidence soon indicated that SiNWs are rod-like structures constructed around a bulk Si single-crystalline core (Holmes *et al.*, 2000; Morales and Lieber, 1998; Teo *et al.*, 2003; Wu *et al.*, 2004; Zhang *et al.*, 2000).

An important consequence of their single-crystal nature is that SiNWs grow along very well defined crystalline directions (see Fig. 2). Wu *et al.* (2004) carried out an interesting and extensive study of the growth orientations, showing a connection between the diameter and the favored crystal axis in the Au-catalyzed synthesis of SiNWs: the smallest-diameter nanowires grow primarily along the $\langle 110 \rangle$ direction, whereas larger nanowires favor the $\langle 111 \rangle$ direction; intermediate diameters, 10 to 20 nm, on the other hand, are dominated by $\langle 112 \rangle$ wires. Thermodynamic models have been proposed to account for this diameter-dependent growth direction (Schmidt *et al.*, 2005; Wang *et al.*, 2006a) with consistent results in good agreement with the experiments, fixing the cross-over from $\langle 110 \rangle$ to $\langle 111 \rangle$ growth at 20-25 nm ($\langle 112 \rangle$ orientation was not considered in those studies). The stacking sequence preference that leads to $\langle 110 \rangle$ over $\langle 111 \rangle$ SiNWs at small diameters is also supported by first-principles calculations (Akiyama *et al.*, 2006). More recently, a continuum model that allows studying how growth begins and evolves toward steady-state wire growth has been presented (Schwarz and Tersoff, 2009). The advantage of this approach is that complex

situations such as catalyst coarsening and interrupted growth can be easily handled.

Ideally, nonetheless, one would like to be able to control the wire orientation at growth time. An important achievement in this sense was the demonstration that the growth orientation can also be controlled externally by adjusting the growth pressure (Holmes *et al.*, 2000; Lugstein *et al.*, 2008). Alternatively, the use of different techniques can bias somehow the growth along certain crystal axis. For instance, the less common oxide-assisted growth method, generally yielding a broader diameter distribution (Wang *et al.*, 1998), might favor different orientations for ultra-thin SiNWs (Teo *et al.*, 2003). Significantly, the thinnest SiNW reported to date (Ma *et al.*, 2003) was synthesized with this technique and was a $\langle 112 \rangle$ wire (see Fig. 3).

B. Surface reconstructions in pristine nanowires

The next major issue one has to face when studying the structure of a SiNW is the shape of its cross-section which, as we shall see briefly, is intimately related with the growth orientation. Although one can pictorially imagine nanowires as cylindrical structures, clearly, when going down to the atomic-scale detail, this is not the structural arrangement that they assume –or even *can* assume. The analogous problem in solids and small particles (Wang *et al.*, 1984; Zhdanov and Kasemo, 1998) is elegantly solved by means of the Wulff construction or Wulff rule (Marks, 1994), which relates the equilibrium shape with the surface free energy of the facets involved. Solving the energy minimization problem $\min \sum s\gamma_s$, where s is the number of surface unit cells and γ_s the corresponding energy, leads to the optimum shape.

Zhao and Yakobson (2003) have reexamined the use of Wulff construction within the determination of the equilibrium cross-sections of SiNWs. They showed that the conventional formulation of the Wulff criterion lacks of two important aspects: (i) in solids and smooth spherical particles the energy of the edges between facets is neglected compared to the surface contribution; (ii) the bulk is assumed already at its minimum and thus invariant. Hence, they propose the following generalization for the Wulff energy:

$$F = E_e + \sum_s s\gamma_s + E_b \quad (1)$$

where they include the energy of matching adjacent facets E_e , i.e. the energy of the edges, and the energy of the bulk E_b , releasing the constraint on the innermost part of the wire

which can now change.

They investigated different faceting arrangements for SiNWs grown along the $\langle 110 \rangle$ axis comparing them on the basis of Eq. 1. They found that the ground-state structure for SiNWs up to 5 nm is a pentagonal cross-section constructed joining five prisms cut out of a $[110]$ Si plane [see Fig. 5(d)]. This structure has seldom been detected experimentally [a remarkable observation by Takeguchi *et al.* (2001) is shown in Fig. 5(e)], probably because it is not constructed around a bulk-core, which seems to be the favored situation at growth time. However, if one restricts to wires with a strictly bulk core the model of Zhao and Yakobson (2003) correctly predicts hexagonal over square cross-sections for $\langle 110 \rangle$ SiNWs, in agreement with the experiments (Ma *et al.*, 2003; Wu *et al.*, 2004) (see Fig. 7).

The most important result of the work of Zhao and Yakobson (2003) is emphasizing the role of the edges and how the interplay between edges and surfaces play a key role in determining the reconstruction of Si one-dimensional structures. Before its formalization, this effect had been already pointed out by Ismail-Beigi and Arias (1998) a few years earlier. In their work they considered a pristine SiNW grown along the $\langle 100 \rangle$ axis. This orientation favors a square cross-section with $\{100\}$ facets, an energetically *cheaper* solution than a square cross-section with $\{111\}$ facets (Rurali and Lorente, 2005b). The abrupt match between the $\{100\}$ facets results in an energetically expensive edge, a large value of E_e in Eq. 1, which can be reduced by forming smaller, transition $\{110\}$ facets that allow a smoother match between the dominant $\{100\}$ facets and partially release the stress accumulated at the edge (examples can be seen in Figs. 4(c), 6(a) and 8.).

Unfortunately, a word of care should be spent concerning the above discussion. Down at the ultimate nanoscale limit it is delicate to give general rules and for extremely thin SiNWs counterexamples can be found to the general trends discussed previously. For instance, Cao *et al.* (2006) showed that the faceting arrangement proposed by Ismail-Beigi and Arias (1998) for $\langle 100 \rangle$ wires and later followed by other authors (Lee and Rudd, 2007b; Rurali, 2005; Rurali and Lorente, 2005a; Vo *et al.*, 2006) is favored only beyond a 1.7 nm diameter, whereas tiny SiNWs prefer sharp edges, i.e. the removal of the edges does not pay back.

In the spirit of the work of Zhao *et al.* (2004), Justo *et al.* (2007) carried out an interesting and systematic study of SiNWs grown along the $\langle 100 \rangle$, $\langle 110 \rangle$, and $\langle 112 \rangle$ crystal axis, carrying out extensive calculations based on an interatomic potential (Justo *et al.*, 1998). In order to elucidate the role of the different facets for the stability, for each growth orientation they

examined cross-sections bounded by different facet compositions. For the $\langle 100 \rangle$ SiNWs, for instance, they considered both all- $\{100\}$ facets, all- $\{110\}$ facets and three intermediate combinations. Proceeding in this way they were able to formulate a universal scaling law in terms of the wire perimeter, according to which the nanowire energy per atom always lies within two limiting energy lines, which are directly related to the character of the prevailing facets. Interestingly, in the limit of thick wires, the edge energy become negligible as suggested by Zhao *et al.* (2004) and the energy scales linearly with the inverse of the wire perimeter.

Silicon has a very rich phase diagram (Kaczmariski *et al.*, 2005) and many solid phases other than the diamond structure are known. Among them is the so-called clathrate phase that becomes stable at negative pressures. The stability of such a phase for quasi one-dimensional nanostructure has been investigated by Ponomareva and co-workers (Ponomareva *et al.*, 2006, 2005). They studied cage-like SiNWs *carved out* of a Si clathrate structure and compared them with both tetrahedral diamond-like and polycrystalline SiNWs. Their results indicate that also in these nanostructures the tetrahedral structure is favored. Nevertheless, the difference in energy is rather small and it is suggested that clathrate based SiNWs might have better conductive properties.

C. Passivated nanowires

The study of the structure of pristine SiNWs has been a fertile ground where to start the theoretical research of these fascinating systems. However, quite soon it became clear that the wires grown experimentally have always *passivated* facets. Silicon form highly directional covalent bonds according to the know sp^3 tetrahedral pattern. Silicon atoms at the surface have dangling bonds (DB), unsaturated bonds that make the atom highly reactive and that induce strong reconstruction of the surfaces. Generally speaking, surface passivation consists of the termination of DBs on the surface with elements that assure their chemical stability. Hence the surface is chemically *passive*.

Surface passivation in SiNWs mainly originates from two causes: (i) the growth of a thin layer of SiO_2 by thermal oxidation of silicon; (ii) presence of hydrogen in the growth environment during the synthesis or HF attack of the oxidized wires after growth, a process yielding removal of the SiO_2 layer and H passivation. Hydrogen passivation is rather simple

to model. If a sufficient amount of hydrogen is supplied the H atoms readily terminate each Si DB by forming a stable Si-H system. Passivation by oxidation is more complex. Thermal oxide is amorphous and then difficult to model at the nanoscale, because of the large amount of atoms required to describe the disordered phase. In the study of SiNWs, for most practical effects, hydrogen termination is a reasonable approximation to oxide passivation and this is the strategy adopted in most of the theoretical studies reviewed here. This approach is also justified by the fact that it is easy to remove the oxide layer after the growth and to induce H passivation by simply etching it with HF. This procedure is often followed (Guichard *et al.*, 2006; He and Yang, 2006; Ma *et al.*, 2003; Ross *et al.*, 2005; Wang *et al.*, 2008; Wu *et al.*, 2004) in order to work with *cleaner* structures where the passivation rely on an individual termination of the DBs, rather than a less controllable and more defective oxide coverage (Baumer *et al.*, 2004). Furthermore, it has also proven to leave the morphology of the nanowire essentially intact, except for the removal of the oxide layer (Zhang *et al.*, 2000), allowing inspection of the underlying atomic scale structure (see Fig. 3). Yet, more attention is likely to be devoted in the near future to the specific nature of SiO₂ passivation, beyond the simple models considered so far (Avramov *et al.*, 2007).

The passivation has a crucial effect on the electronic structure of the wires and it is essential to provide the wires with predictable band gap widths and an invariably semiconducting character. We will discuss these topics in detail in Section III.

Surface passivation has also an important effect on the structural arrangements of SiNWs. Besides preventing complex reconstructions, it also influences the structure of the sub-surface and innermost part of the wires. H-passivated SiNWs grown along different orientations have been found to maintain remarkably the bulk symmetry (see Fig. 4), with negligible deviations of the Si-Si bond lengths; the deviation increases close to the surface, depending on the level of surface rearrangement (Vo *et al.*, 2006). The limit case in this sense are pristine wires, where the absence of passivation results in major surface rearrangements and large deviations of the Si-Si bond length also in the wire core (Kagimura *et al.*, 2005).

An interesting path to the determination of the structure of H-passivated $\langle 110 \rangle$ SiNWs has been proposed by Chan *et al.* (2006). Their optimization procedure is based on a genetic algorithm. With this method, in principle suitable for any other growth orientation, they

identified a pool of *magic* structures⁴ for $\langle 110 \rangle$ wires. Although some of them have not been observed experimentally, their hexagonal structure provided a good agreement with the STM image of the wire facet of Ma *et al.* (2003).

A more systematic approach was followed by Zhang *et al.* (2005) in a study analogous to the one performed by Justo *et al.* (2007) for pristine nanowires. They carried out a comprehensive study of the possible low-index facets in H-passivated SiNWs grown along the $\langle 100 \rangle$, $\langle 110 \rangle$, $\langle 111 \rangle$, and $\langle 112 \rangle$ axis. While many choices are possible for $\langle 100 \rangle$, $\langle 110 \rangle$, and $\langle 111 \rangle$ wires, they showed that there is only one low index configuration –with two $\{111\}$ and two $\{110\}$ facets– for $\langle 112 \rangle$ wires. It is suggested that this would ease the controlled growth with a predetermined cross-section and could have important consequences on the engineering of devices based on SiNWs. In Section III.B, however, we will see that it has been recently suggested that the exact cross-section shape is less important than other parameters –such as the effective diameter and the surface-to-volume ratio– when it comes to determining the electronic properties of SiNWs.

Another important aspect to consider in H-passivated SiNWs is the surface structure of the hydrogenated facets. This issue has been tackled by Vo *et al.* (2006), where a systematic study of the effects of varying the diameter and the growth direction has on the structure of the hydrogenated surfaces of $\langle 100 \rangle$, $\langle 110 \rangle$ and $\langle 111 \rangle$ SiNWs. In particular, they studied the relative stability of symmetric SiH_2 dihydrides, canted SiH_2 dihydrides and a (2×1) surface reconstruction (where first reconstruction is allowed and then passivation occur), see Fig. 6. They deliberately chose simple, round cross-sections, as their scope was focusing on the atomic scale structure of the facet. Their wires were constructed selecting all the atoms falling inside a virtual cylinder placed in bulk silicon, in such a way that the facets approximated a circular cross-section. This procedure agrees with the smoothness prescription described above, which –more importantly– seems also to be confirmed by the experiments (Ma *et al.*, 2003). They found that, in agreement with bulk Si(100) surfaces (Northrup, 1991), the canted dihydride surface is more stable than the symmetric dihydride structure, because canting allows a larger H-H separation. Additionally, faceting confers an increased stability to the canted dihydride surface, because at the facets' edges the

⁴ *Magic* structures is used in this context to refer to distinct types of wire configurations with low formation energies that emerge as the number of atoms per length is increased (Chan *et al.*, 2008).

SiH₂ groups are free to rotate. Relief of the surface strain through bending as an additional mechanism has been explored by Zdetsis *et al.* (2007).

A perhaps more flagrant effect of the surface induced strain is the fact that the axial lattice parameter of thin SiNWs is in general different from bulk Si. Ng *et al.* (2007) reported contraction along the wire axis for $\langle 100 \rangle$, $\langle 111 \rangle$ and $\langle 112 \rangle$ SiNWs, and elongation for $\langle 110 \rangle$ growth orientation.

Other types of surface passivation –including OH (Aradi *et al.*, 2007; Ng *et al.*, 2007; Nolan *et al.*, 2007), NH₂ (Nolan *et al.*, 2007), F (Ng *et al.*, 2007), or Br, Cl, and I (Leu *et al.*, 2006)– have been considered. While changing the passivation has a limited effect the structural properties of the nanowire, it can affect in a more significant way the electronic band structure. We will come back on this topic in Section III.B.3.

As a conclusive remark one should notice that, despite the intensive research carried out to find the equilibrium shapes for the different growth orientations –proposing structures that range from fullerene-like (Marsen and Sattler, 1999) to star-shaped (Sorokin *et al.*, 2008)– in most cases the experimentally observed cross-sections of passivated SiNWs are deceptively simple (see Fig. 3 and 7), whereas unpassivated SiNWs have never been reported. Furthermore, as we shall see in Section III, although the cross-section shape has captured great attention and has been the object of many studies, in realistic, passivated wires the growth orientation and the average diameter turned out to have a more significant impact on the electronic properties of SiNWs.

D. Mechanical properties of nanowires

If one *carves out* of bulk Si a rod-shaped system like a nanowire, there is no apparent reason to expect an enhanced stiffness, while the larger surface-to-volume ratio is rather suspected to be detrimental. A simple way of understanding these effects is that there is a layer of material at the surface and edges whose mechanical properties differ from those of the bulk including different elastic moduli and eigenstrains.

These intuitive ideas have been rigorously tested by Lee and Rudd (2007b), by means of an exhaustive study of $\langle 100 \rangle$ SiNWs with increasing diameters. They calculated the Young’s modulus, finding that it softens from the bulk value as the surface-to-volume ratio increases, going through a steep decrease around 2-2.5 nm diameter (see Fig. 8). They

showed that the origin of this behavior is the compressive surface stress. To get a better insight into these atomic scale mechanisms the Young's modulus can be decomposed into a core (Si core atoms) and a surface contribution (Si surface atoms, H-H and Si-H systems). This decomposition allows highlighting the insensitivity to the facet ratio, as the contributions to the Young's modulus that are strongly facet dependent are very small. These first-principles results are in good agreement with empirical atomistic potentials and continuum techniques (Lee and Rudd, 2007a), unless for the smallest wires where these simplified approaches fail (see Fig. 8).

The Young's modulus, as many other properties of ultra-thin SiNWs reviewed in this paper, is strongly anisotropic. Ma *et al.* (2008) extended the study of the stiffness vs. diameter to wires grown along the $\langle 110 \rangle$, $\langle 111 \rangle$, and $\langle 112 \rangle$ orientations. While their results are in good agreement with those of Lee and Rudd (2007b) for $\langle 100 \rangle$ wires, they showed that wires of similar diameter, but with different orientations, differ considerably. In particular they found the highest values for $\langle 110 \rangle$ SiNWs, while $\langle 100 \rangle$ SiNWs give the lowest values. These results are in good agreement with the work of Leu *et al.* (2008) where the Poisson ratio is also considered.

We note that to calculate the Young's modulus a definition of the cross-sectional area must be assumed and it is not univocal. We will run into a similar problem concerning the definition of the wire diameter in Section III.B.2 when dealing with quantum confinement. Lee and Rudd (2007b) took the area bounded by the outermost atoms, i.e. the passivating H atoms, Ma *et al.* (2008) made a similar choice, but excluding the H atoms. Aware of this degree of arbitrariness in the possible choices, Leu *et al.* (2008) studied the variation of the calculated mechanical properties as a function of the uncertainty δr_0 in the estimation of the radius r_0 . The error in the Young's modulus is $2\delta r_0/r_0$ and goes to zero in the limit of large wires ($r_0 \rightarrow \infty$). The Poisson ratio, on the other hand, is much more sensitive, because the error is $-\delta r_0/r_0 + (\delta r - \delta r_0)/(r - r_0)$, r being the radius at a strain ϵ ; while the first term vanishes for large radius, the other is always present and can be significant as $(r - r_0)$ is typically small.

Bending has received comparatively less attention, although a few experimental measurements have been reported (Hoffmann *et al.*, 2006; Hsin *et al.*, 2008; Tabib-Azar *et al.*, 2005; Zheng *et al.*, 2009). This is probably due to the difficulty of studying a bended nanowire within atomistic simulations that normally relies on periodic boundary conditions. The fab-

rication of ingenious mechanical structures with enhanced elastic properties suggests that this could be a promising research direction (San Paulo *et al.*, 2007).

Beyond elastic deformation, materials undergo non reversible, plastic deformation which directly precede fracture. This regime has been studied for $\langle 100 \rangle$ pristine SiNWs (Justo *et al.*, 2007) and for $\langle 111 \rangle$ and cage-like SiNWs (Menon *et al.*, 2004), using two different interatomic potentials (Justo *et al.*, 1998; Stillinger and Weber, 1985). At small strains ϵ the stress increases linearly, as expected in the elastic regime, while at larger deformation the plastic behavior appears until the fracture occurs at $\epsilon \sim 0.10$, with a good agreement between the two different models. Experimentally, however, the fracture is much delayed with respect to theoretical predictions and the wire breaks at $\epsilon \sim 0.25$ (Kizuka *et al.*, 2005). It should be mentioned that both these theoretical studies considered pristine nanowires, while the wires in the experiments are coated with a thin layer of oxide, thus it is difficult to make a rigorous comparison. At the same time it is not surprising that a different surface treatment can produce a noticeable difference in the mechanic response, because it is just at the surface that the nanoscale signature emerges.

Correlating structural deformations and changes in the electronic properties is an active field of research (Rurali *et al.*, 2008a) and the use of strain to enhance carrier mobility has been investigated (Hong *et al.*, 2008; Huang *et al.*, 2008; Leu *et al.*, 2008). Furthermore, a giant piezoresistance effect –the application of a strain to a crystal that results in a change in the electrical resistance– has been reported recently (He and Yang, 2006). The underlying atomic scale mechanism is still poorly understood, however, and the attempts made so far proved to be somehow elusive (Cao *et al.*, 2007; Rowe, 2008).

III. ELECTRONIC PROPERTIES

A. Pristine Nanowires

The reason for the attention devoted to geometrical features such as the growth orientation, the faceting arrangement, and the surface structure, is that they are crucial when it comes to the electronic properties of the nanowire. Clearly, the thinner is the nanowire, the more it is sensitive to the structure details, as in the limit of very large diameter –no matter which is its crystal axis or cross-section shape– its properties converge to those of bulk Si.

As we discussed in the previous section, pristine nanowires turned out to have a limited relevance, at least to date, because experimentally grown SiNWs are always passivated. However, the study of bare, unpassivated wires is still interesting for two reasons: (a) it leads to the important conclusion that passivation is essential to obtain nanowires with predictable and easy to control electrical properties; (b) it sheds a light on some atomic scale mechanisms of high fundamental interest.

An interesting example in this sense is the electronic structure of $\langle 100 \rangle$ SiNWs with $\{100\}$ facets. While other facets, like the $\{111\}$ facets, have an electronic structure similar to the corresponding infinite surface (Pandey, 1981; Rurali *et al.*, 2006), $\{100\}$ facets can be very different. In the Si(100) surface each surface atom has two DBs. The surface is known to reduce its energy by forming dimers, thus halving the number of DBs (Chadi, 1979). The reconstruction of $\{100\}$ facets follows the same pattern, but wires dominated by such facets have been reported to be metallic. Rurali and Lorente (2005a) showed that thin $\langle 100 \rangle$ SiNWs sustain two different reconstructions of the $\{100\}$ facet that turn the wire metallic or semimetallic, in agreement with what previously suggested by Ismail-Beigi and Arias (1998). The metallic behavior can be ascribed to a modified coordination of the $\{100\}$ facet atoms, leading to a distortion of the surface dimers, with respect to the Si(100) surface (Rurali *et al.*, 2006). The metallicity rapidly vanishes as the diameter is increased and the facets recover the coordination and the semiconducting electronic structure of the Si(100) surface.

The $\langle 100 \rangle$ wires with sharp corners studied by Cao *et al.* (2006) can be metallic too. Interestingly, the edge metallic states decay slower with the diameter compared to the facet metallic states. Consequently, wires thicker than those considered by Rurali and Lorente (2005a), where edges were absent, can still be metallic. In both cases the metallic states are related directly or indirectly with the edges –in one case purely edge states, in the other dimer rows with an altered coordination near the edges; as the wire size increases the relative number of atoms at the edges decreases rapidly and the facet recovers the semiconducting character of the infinite surface.

Besides the fundamental interest of these findings –in one case a metallicity driven by the finite size of the facet, in the other sustained by the edges– it is clear that such wires are not desirable for electronics application. On the one hand one wants to work with semiconducting systems; on the other hand, although some application can be envisaged for metallic SiNWs, e.g. interconnects, the metallicity should be much more robust, so that it

is not destroyed by small variations of the diameter and does not depend critically on the atomic scale structure of the wire.

A comprehensive study of the surface reconstruction and electronic structure of pristine $\langle 110 \rangle$ wires has been carried out by Singh *et al.* (2005). The cross-section chosen for these wires is such that they have $\{100\}$ and $\{110\}$ facets, at variance with the SiNWs of Rurali *et al.* (2006) which have $\{111\}$ and $\{110\}$. This variation results in significant structural differences, because of the comparatively larger readjustment of $\{100\}$ facets, which involve the formation of surface dimers (Chadi, 1979) and therefore a noticeable reconstruction; in $\{110\}$ and $\{111\}$ facets, on the other hand, no new bonds are formed and the overall reorganization of surface atoms is moderate. These $\langle 110 \rangle$ SiNWs turned out to be indirect band gap semiconductors, with the states of the top of the valence band and the states of the bottom of the conduction band originating at different facets. Yet, it should be noted that a metallic reconstruction for $\langle 110 \rangle$ SiNWs have been reported by Fernández-Serra *et al.* (2006b). Once again, small variations of the atomic scale structure or of the cross-section can result in major changes in the electronic structure.

Contrarily to what we shall discuss in Section III.B.2 concerning quantum confinement, here the thinner is the wire, the smaller is the effective band gap. This looks like a general feature of pristine, unpassivated nanowires, where band gaps are smaller than in bulk (Rurali, 2005; Rurali *et al.*, 2006). In thin wires the surface-to-volume ratio is larger and surface states, which often lie in the gap, dominate the electronic structure and result in an effective narrowing of the energy gap.

B. Passivated nanowires

1. Band structure and band gap anisotropy

We have already mentioned a few times that surface passivation is required to obtain ultra-thin nanowires that are semiconducting and have a predictable and controllable band gap. Notwithstanding, the electronic structure of the nanowires still depends on the growth orientation, on the cross-section shape and on the diameter. The band gap is strongly anisotropic (Leu *et al.*, 2006, 2008; Ng *et al.*, 2007; Niquet *et al.*, 2006; Rurali *et al.*, 2007a; Singh *et al.*, 2006; Vo *et al.*, 2006; Yan *et al.*, 2007; Zhao *et al.*, 2004) and, for wires of com-

parable diameters, it follows the ordering

$$E_g^{\langle 100 \rangle} > E_g^{\langle 111 \rangle} \sim E_g^{\langle 112 \rangle} > E_g^{\langle 110 \rangle}, \quad (2)$$

with the orientation effect still sizeable up to 3 nm diameter (Ng *et al.*, 2007). The band gap of $\langle 112 \rangle$ wires is of the same order of $\langle 111 \rangle$ wires, though it has been reported to be slightly larger (Leu *et al.*, 2006; Rurali *et al.*, 2007a) or slightly smaller (Ng *et al.*, 2007). This anisotropy has been qualitatively tracked back to the different geometrical structure of the wires in the $\langle 100 \rangle$, $\langle 111 \rangle$, and $\langle 110 \rangle$ directions (Bruno *et al.*, 2005, 2007b). While the $\langle 100 \rangle$ and $\langle 111 \rangle$ wires appear as a collection of small clusters connected along the axis, the $\langle 110 \rangle$ wires resemble a linear chain (see Fig. 11 where the case of Ge nanowires is shown). Therefore, one expects that quantum confinement effects are larger in the $\langle 100 \rangle$ and $\langle 111 \rangle$ wires, because of their quasi zero-dimensionality, with respect to the $\langle 110 \rangle$ wires.

Bulk Si has an indirect band gap, with the valence band maximum at the Γ point and the conduction minimum at about 85% along the Γ to X direction, and a phonon is required to conserve the momentum in any electronic transition. Remarkably, however, SiNWs grown along most of the crystallographic orientations have a direct band gap, meaning that the maximum of the valence band and the minimum of the conduction band occur at the same point in k -space. This property has allowed to envisage the use of SiNWs as optically active materials for photonics applications (Canham, 1990; Guichard *et al.*, 2006).

In $\langle 100 \rangle$ SiNWs, the confinement plane contain four of the six equivalent conduction band valleys. These minima at $\pm y$ and $\pm z$ are then projected onto Γ due to band folding, thus resulting in a direct band gap. When the axis is along a lower symmetry direction the confinement plane cannot contain four conduction band valleys and it will contain at most two. This is the case of $\langle 110 \rangle$ SiNWs. The minima at $\pm z$ are projected onto Γ again. Now, both the large and the small masses appear in the confinement plane, with the larger longitudinal mass being the relevant effective mass for describing the confinement effect in the cross-section plane. On the other hand, the four remaining minima will be projected to a point between Γ and the zone boundary Z, with the effective mass on the confinement plane being a value between the longitudinal and transverse masses. Therefore, the conduction-band edge at Γ is expected to have a smaller upward shift induced by confinement and the band gap becomes direct (Yan *et al.*, 2007).

Although the projection along the $\langle 111 \rangle$ axis would lead to an indirect band gap,

the thinnest $\langle 111 \rangle$ SiNWs have a direct band gap (Rurali *et al.*, 2007a; Vo *et al.*, 2006; Zhao *et al.*, 2004). One should bear in mind that, besides the band folding arguments given above, the effective masses play an important role. In the quantum confinement regime (see below, Section III.B.2) the conduction band states are shifted upward, the smaller the diameter, the larger the shift. Nonetheless, the magnitude of this energy shift is different for each k -point of the band structure and depends on the effective mass. In bulk Si the effective mass at Γ is heavier than at X or L . Hence, upon confinement, one expects the conduction band energy at X and L to increase more than at Γ . This simple considerations based on effective mass theory (EMT) describe well the transition from direct to indirect band gap experienced by $\langle 111 \rangle$ SiNWs that occur around 2 nm: as the diameter increases the quantum confinement effect vanishes (see Section III.B.2), Γ and X and L points are not shifted and the gap remains indirect. Among the studied orientations $\langle 112 \rangle$ SiNWs are the only ones that have an indirect band gap also for the thinnest diameters (Aradi *et al.*, 2007; Huang *et al.*, 2008; Lu *et al.*, 2008a; Ng *et al.*, 2007; Rurali *et al.*, 2007a; Scheel *et al.*, 2005).

Although the band gap is highly anisotropic and, as we shall see in the next section, strongly dependent on the wire diameter, it is very interesting to observe that it is rather insensitive to the shape of the cross-section. Ng *et al.* (2007) have studied the effect of the variation of the cross-section in thin $\langle 110 \rangle$ SiNW, generating 13 different cross-sections obtained by modifications of a reference 1 nm wire. They found that the band gap is practically constant and changes are within 0.09 eV. Later, it was demonstrated that wires of even utterly different cross-sections can have the same band gap, provided that their surface-to-volume ratio is the same (Yao *et al.*, 2008). The effect of the surface-to-volume ratio on the band gap can be described by the universal expression

$$E_{gap} = E_{gap}^{bulk} + aS \quad (3)$$

where E_{gap}^{bulk} is the gap of bulk Si, a is an adjustable parameter and S is the surface-to-volume (in nm^{-1}).

2. Quantum confinement

One of the most intriguing physical effect that arise in confined systems like SiNWs is the so-called *quantum confinement*. Such a regime is conveniently described through the particle-in-a-box model system in most quantum mechanics text books (Bransden and Joachain, 2000). The simplified situation considered is an infinite potential well where the motion of the particles is restricted to be in the direction of the confinement. As the motion of the particles is restricted, their kinetic energy increases and it is readily shown that the eigenstate energies are given by the following relation:

$$E_n = \frac{\hbar^2 n^2 \pi^2}{2m^* d^2} \quad (4)$$

where m^* is the effective mass and d the width of the potential well. According to Eq. 4, not only the energy levels, but also the spacing between them increases as the confinement becomes more pronounced, i.e. the smaller is d . Quantum confinement has a critical impact on semiconductors because it affects directly their most important electronic property: the energy band gap.

Semiconducting nanowires provide a very good approximation of the model situation described above. Clearly, the potential well is not infinitely deep and realistic wire cross-sections like those described in Sections II.B and II.C are difficult to describe analytically, thus there is a need for a detailed electronic structure modeling.

The first experimental proofs of quantum confinement in nanostructured Si were reported in the pioneering works of Canham (1990) and Lehmann and Gösele (1991), where a simple electrochemical etching process was used to create crystalline Si nanostructures with visible luminescence at room temperature. As TEM images revealed later (Cullis and Canham, 1991), the etched structures consisted of rather disordered bundles of nanowires, though it is interesting to note that ordered structures like those speculated in the first place (Canham, 1990) have been recently proposed for the fabrication of ordered arrays of quantum wires (Rurali *et al.*, 2007b) and to achieve enhanced thermoelectric effect (Lee *et al.*, 2008).

Read *et al.* (1992) and Buda *et al.* (1992) performed DFT calculations of the band gap upshifts in perfect H-terminated SiNWs as a function of wire thickness, modeling porous Si (Canham, 1990) with rectangular columns oriented along the $\langle 100 \rangle$ axis. Both these works showed that the fundamental gap is direct at the Γ point. This makes by itself the probability

of radiative recombination higher than in bulk Si, since no phonon is required in the electron-hole recombination process. Unfortunately, as it is well-known, standard local and semi-local implementations of DFT fail to account quantitatively for the band gap of semiconductors and one must resort to self-energy corrections to the Kohn-Sham gap to obtain a good agreement with the experimental values. Yet, the trends are expected to be qualitatively correct (Williamson *et al.*, 2002) and Read *et al.* (1992) reported band gap upshift of up to 2 eV for wires of ~ 12 Å diameter. They also shown that a generalization of Eq. 4 gives a good description of the quantum confinement for wires wider than 23 Å, whereas thinner wires show significant deviations from this idealized EMT picture. In such a range Buda *et al.* (1992) showed that with the more realistic DFT potential the band gap scales as the inverse of the diameter d , rather than $1/d^2$ as predicted by particle-in-a-box arguments where infinitely hard walls are assumed. Subsequent studies that the interested reader could look at include the works by Ohno *et al.* (1992), Sanders and Chang (1992), Hybertsen and Needels (1993), Xia and Chang (1993), Yeh *et al.* (1994), Saitta *et al.* (1996), Xia and Cheah (1997), and Ossicini *et al.* (1997).

A first step toward a quantitative evaluation of SiNW band gaps in the quantum confinement regime was given by Delley and Steigmeier (1995), including a constant self-energy correction independent on the size. Namely, they increased all their calculated band gaps by 0.6 eV, the self-energy correction for bulk Si. They also shown that EMT can predict with great accuracy the band gap of relatively thin nanowires, provided that the potential well is not assumed to be infinite.

The self-energy correction to the Local Density Approximation (LDA) or the Generalized Gradient Approximation (GGA) band-gap, however, is expected to depend on the wire diameter and on the growth orientation. Zhao *et al.* (2004), Bruno *et al.* (2007a), and Yan *et al.* (2007) carried out calculations within the many-body perturbation method based on the GW approximation (Aryasetiawan and Gunnarsson, 1998) for $\langle 100 \rangle$, $\langle 110 \rangle$, and $\langle 111 \rangle$ SiNWs. They showed that the self-energy is indeed anisotropic and is larger for thinner wires. The dependence of the band gap on the wire diameter can be described as

$$E_{gap} = E_{gap}^{bulk} + C \times (1/d)^\alpha, \quad (5)$$

where E_{gap}^{bulk} is the calculated band gap of bulk silicon, d is the effective diameter of the wires, while C and α are fitting parameters. This formula is derived within a simple particle-in-

a-box effective mass approximation, where $\alpha = 2$ when barrier height is infinite. The GW results can be fitted to this formula, yielding values of α ranging from 0.9 to 1.1, much lower than those expected within EMT and depending on the growth orientation (see Fig. 10), so that the band gap and the dielectric response are anisotropic (Bruneval *et al.*, 2005; Bruno *et al.*, 2007a; Zhao *et al.*, 2004).

Although GW is in principle the best suited methodology to calculate the band gap in semiconductor systems, it suffers from the serious inconvenience of a considerable computational load. In the works of Zhao *et al.* (2004), Bruno *et al.* (2007a) and Yan *et al.* (2007), for instance, only relatively small SiNWs can be calculated directly and the band gaps of larger, more realistic wires are obtained by numerically fitting the available data to Eq. 5. Furthermore, an alternative to many-body GW calculations is mandatory when it comes to calculate doping levels, a task that requires large computational cells. In the remainder of this section we discuss two possible approaches.

A successful way to improve the DFT band gaps consists in using hybrid-functionals for the exchange-correlation energy, where a certain amount of exact Hartree-Fock exchange is mixed to conventional LDA/GGA functionals. The amount of Hartree-Fock exchange (typically 12-15%) is chosen to reproduce some parameters of the bulk system (the band gap, among them), rather than being based on solid theoretical grounds. Hence, strictly speaking, one cannot claim to solve the electronic structure *from first-principles*. In such a theoretical framework the band gap of SiNWs with diameters up to 3 nm can be calculated directly (Aradi *et al.*, 2007; Ng *et al.*, 2007; Rurali *et al.*, 2007a). These results are important because they allow *direct* comparison with the only experimental measurements available to date (Ma *et al.*, 2003). A direct comparison of the experimental data with GW calculations is not possible for two reasons: the diameters of the wires grown experimentally are larger than those that could be simulated and most of the available measurements are for $\langle 112 \rangle$ SiNWs, whose larger primitive cell precludes GW calculations even for the thinner wires.

Alternatively, the band structure of nanowires can be calculated with a semiempirical tight-binding method, where the self-energy is obtained within a simpler semiclassical treatment of the image charge effects (Niquet *et al.*, 2006). This is a very powerful method because, due its reduced computational load, it allows calculating SiNWs with diameters up to 10 nm with good accuracy. As we will see in some more detail below (Section III.C.3), a

great advantage of this method is that it allows dealing with different dielectric surroundings, which is very important in systems with abrupt dielectric interfaces like nanowires (Li *et al.*, 2008).

So, how should the band gap of SiNWs be calculated? The accurate calculation of band gap is one of the most challenging problems in semiconductor theoretical physics, so it is not surprising that it is not easy to answer this question. GW calculations provide in principle the most accurate estimations. However, they are restricted to very thin SiNWs. Semiempirical tight-binding, on the other hand, is a very attractive choice for larger wires, especially for those diameters where quantum confinement become small and gap broadening is dominated by dielectric mismatch effects (Pereira *et al.*, 2009). Hybrid-functional DFT calculations are an interesting compromise for those wires that are too large for GW (too many atoms in the primitive cell) and too small for tight-binding (relaxation effects cannot be neglected and the use of a parametrization obtained for bulk Si could be questioned). It is difficult to asses on the accuracy of each of these methods, since the experimental measurement of the energy gap of SiNWs is extremely challenging, and only the data of Ma *et al.* (2003) are available to date. More experimental results are needed to clarify this important point.

3. Surface chemistry

We have seen above –and will see again below– that many properties of SiNWs are determined by their large surface-to-volume ratio. Hence, it is natural that most of the exciting physics takes place at the wires’ surface (Kobayashi, 2004; Zhong and Stocks, 2006). In Section III.A we have seen, for instance, that wires bounded by facets derived by semiconducting surfaces can exhibit surface metallicity. Passivated nanowires are more predictable, in this sense, and it is just because they are always semiconducting that they are expected to play an important role in the next generation of electronic devices. Yet, the surface has a relevant role that merits some considerations.

An important case is that of chemical sensors where the adsorption of a molecule yields measurable variations of the electrical conductance (Blase and Fernández-Serra, 2008; Cui *et al.*, 2001b). Upon adsorption, the molecular orbitals can hybridize with the wire states, resulting in a sizeable modifications of its electronic structure. Whether the ef-

fectiveness of this process depends on the facet where adsorption takes place is the topic addressed by Leão *et al.* (2007). They studied the sensitivity of different facets of a $\langle 110 \rangle$ SiNW, showing the existence of a specific relation between the way surface atoms are bonded to core atoms and the relative contribution of these surface atoms to band edge states. These observations are important concerning the optimal design of those chemical sensors where the adsorption of a molecule directly modify the wire transmission. A broader class of sensors, however, seems to work on simpler basis. The dipole induced by molecule adsorption can act as a gate voltage, opening or closing the conductive channel in a field-effect transistor set-up.

In the quantum confinement regime the band gap width depend critically on the diameter. The possibility of controlling the band gap width is tremendously attractive for optoelectronics applications: not only SiNWs can have a direct band gap, which *per se* increases the optical efficiency, but its width can in principle be tuned. It is not difficult to imagine, however, that controlling the wire diameter with tolerances within 1-3 nm is a more than challenging task. A simpler route to band gap tuning is controlling the chemical composition and the coverage density of the wire surface. Halogens such as Cl, Br, and I can be used as surface passivation agents instead of H and, while not altering the semiconducting character of the wires, they result in a significant shrinking of band gap (Leu *et al.*, 2006). The strongest reduction of the band gap is provided by I, followed by Br and Cl, in the opposite order of the bonding strength of these species and SiNWs. Interestingly, the surface coverage is a further degree of freedom and one can span all the band gap values between a H- and halogen-passivated wire by varying the H:halogen ratio. Also, increasing the halogen surface concentration the band edge states, concentrated in the wire core in presence of H-passivation, progressively spread to the surface.

Analogous results have been reported for OH and NH₂ (Aradi *et al.*, 2007; Nolan *et al.*, 2007). It should be noted that the passivating species do not contribute significantly to the states close to the band edges, so that the reduction of the gap is not caused by the introduction of additional bands. It rather comes from the hybridization of the valence band states with the frontier orbitals of the different passivating functional groups that cause a significant band gap reduction relative to H-passivated wires.

These results indicate that the band gap width in SiNWs can be tailored not only by controlling the wire diameter, but also by an appropriate choice of the surface termination.

C. Doped and defective nanowires

Semiconductors are privileged materials for electronics applications because their resistivities can be varied by design with great control⁵. Equally important, they can be designed to conduct one of two types of carriers: electrons and holes. These two features are the core of device design, which relies on the interaction of adjacent semiconductors with different densities of electrons and holes. The most efficient way to control the carrier density is *doping* the semiconductor, that is incorporating substitutional impurities (*dopants*) in the lattice (Muller and Kamins, 1986).

In the simplest model, a substitutional defect with minor relaxation effects forms four bonds with the neighbor atoms in the Si crystal. For a group-V element, such as P or As, the fifth valence electron is not covalently bonded to near neighbors and it is only weakly bonded by the excess positive charge of the impurity nucleus. Hence, a small amount of energy is required to break this weak interaction and this electron is free to wander about the crystal and contribute to conduction. These impurities are called *donors* because they *donate* an electron; analogous arguments apply to group-III elements which are *acceptors*.

There are at least two reasons that make the physics of impurities in nanowires different with respect to bulk systems: (i) the lattice sites are no longer equivalent in the direction of confinement and (ii) in the quantum confined regime all the eigenstates, including those associated to defects, are shifted in energy with important consequences on the dopant activation. Below, we discuss in some detail these and other topics relevant to dopant efficiency. We conclude the section with a generalization of the formation energy for defects in nanowires.

1. Surface segregation, surface traps and dopant aggregation

In bulk Si all the lattice sites are equivalent. In a nanowire this is true only for the axial direction, because the lateral confinement breaks the translational symmetry. In other words, given one arbitrary Si atom in the nanowire, as one moves along the wire axis he finds

⁵ Conventionally, materials with resistivities less than about $10^{-2} \Omega \text{ cm}$ are considered *conductors* and materials with resistivities greater than about $10^5 \Omega \text{ cm}$ are considered *insulators* (Muller and Kamins, 1986).

an infinite number of equivalent atoms, whereas as one moves along the radial direction he finds a finite number of nonequivalent atoms. Therefore, the substitutional defects at these non-equivalent sites will have in general different formation energies and doping levels.

This problem was first tackled by Fernández-Serra *et al.* (2006b), who studied B and P substitutional in $\langle 100 \rangle$ and $\langle 110 \rangle$ SiNWs. They revealed a tendency to surface segregation of these impurities, which means that substitution close to the surface is energetically cheaper than substitution in the innermost part of the wire. The effect is especially pronounced in presence of DB defects, so that the dopant impurities are effectively trapped by these surface defects. Most importantly, the dopant-DB complex is electrically inactive, reducing the carrier concentration at room temperature.

The segregation energy of P is significantly larger than that of B. This means that for the same impurity concentration, a much larger fraction of P atoms will be captured and neutralized by surface traps, resulting in a lower conductance. This is in agreement with the experimental results (Cui *et al.*, 2000; Yu *et al.*, 2000) where, for similar doping levels, B-doped SiNWs present a lower resistance than P-doped ones. Similar studies have been carried out for $\langle 110 \rangle$ SiNWs of different diameters (Leão *et al.*, 2008; Peelaers *et al.*, 2006). They showed that B and P prefer to sit at edge or near edge sites (the most external lattice sites with all-Si nearest neighbors), depending on the surface facet and on the atomic surface structure (Leão *et al.*, 2008).

In perfectly passivated wires the surface segregation originates from a simple *relaxation effect*. At these edge and near edge positions it is easier to release the strain induced by the substitution, whereas in the center of the wire the allowed relaxation is smaller due to the constraint of the surrounding Si lattice. In surface defective wires, on the other hand, the presence of DBs greatly enhances the tendency to surface segregation, with the impurity atoms moving at surface sites. Here the driving force to surface segregation, yielding a much more sizeable effect, is an *electronic effect*: the formation of a stable dopant-DB complex.

The surface trapping of dopants has a dramatic impact for two reasons: (a) the impurities trapped at the surface are deep-state defects and are electrically inactive, thus not contributing to the carrier concentration at room temperature; (b) due to their large surface-to-volume ratio and considering a typical dopant concentration of $5 \times 10^{18} \text{ cm}^{-3}$ and an estimate of 10^{12} cm^{-2} interface DB defects, one finds that for wires of less than 4 nm diameter there are always enough DBs to trap all the dopants (Peelaers *et al.*, 2006). Luckily, the difference in

formation energies among surface and core substitutional sites has been shown to decrease rapidly as the diameters grow larger (Leão *et al.*, 2008). Hence, there is a twofold benefit in enlarging the wire diameter: on the one hand, the surface-to-volume ratio decreases, and so does the density of DBs with respect to the dopants concentration; on the other hand, the trapping efficiency of these reduced density of surface defects is lower, as the formation energies of core substitutionals and dopant-DB complexes become of the same order. Leão *et al.* (2008) estimate that the populations of core and surface dopants will be similar for wires with diameters of 3 nm or more.

The importance of surface impurities has been further highlighted by Durgun *et al.* (2007a). They considered various impurities such as Al, Ga, C, Si, Ge, N, P, As, Te, and Pt, focusing on adatoms configurations, rather than on substitutionals. They found that the energetically most favorable adsorption site of the six considered depends on the group of the Periodic Table that the impurity belongs to. All the configurations studied, however, give rise to deep state in the gap and are not viable choices as active dopants.

Another source of dopant deactivation is the formation of electrically inactive dopant complexes. Two nearest neighbor dopants can form a bound state, so that the weakly bonded electrons that contributed to the conductance are now participating in the dopant-dopant bond. Yet, this energy gain has to compete with the energy cost that results from the strain accumulated around the dopant-pair defect. This strain is more easily released in nanowires than in bulk, due their large surface-to-volume ratio. Moon *et al.* (2008) reported a high stability of P pairs, which increases as the wire diameter is reduced. Interestingly, this is not the case of B. When two B atoms occupy nearest neighbor sites the lattice undergoes a significant relaxation, the B impurities move far apart and assume a planar threefold coordinated configuration. This is possible because, unlike P, B can present either sp^2 or sp^3 hybridization. Again, p -type doping seems to be more robust than n -type doping, at least as far as one considers B and P. A similar mechanism leads to mutual passivation when both a B and a P impurity are present at the same time. Besides the obvious compensation of having an n - and a p -type dopant, Peelaers *et al.* (2006) showed that these impurities favor aggregation at the wire surface. Also, the use of B/P co-doping has been proposed to reduce in a controllable way the band gap (Iori *et al.*, 2008).

2. Quantum confinement

In Section III.B.2 we have seen how one of the most important quantities of a semiconductor, its band gap, depends critically on the wire diameter in the regime of quantum confinement. This is a very important parameter, because it determines the amount of carriers –*intrinsic* carriers– that can be thermally excited from the valence band to the conduction band. Intrinsic carriers, however, are not very important at typical device operation temperatures and the conduction is dominated by *extrinsic* carriers, those carriers that are thermally excited from a dopant level. Hence, dopants to be such must be very *shallow*, meaning that the impurity electronic states have to be only a few meV from the band edge.

Now, if the band gap broadens as an effect of quantum confinement, what happens to dopant levels? In a purely effective mass picture they will be shifted, like any other state, becoming deeper, i.e. the upshift of a donor level will be less than of the conduction band edge. Clearly, this fact has dramatic consequences on the dopant efficiency. Namely, a dopant impurity which is known to be very shallow in bulk Si, becomes deeper as the diameter shrinks down, and it will not eventually be usable to dope ultra-thin SiNWs. At which diameter does this happen?

From EMT, one can deduce the *effective* Bohr-radius of the ground state $a_B \approx (\epsilon/m^*)a_0$, where a_0 is the Bohr-radius of the isolated hydrogen atom. This results in about 2.2 nm (thus a 4.4 nm diameter) for P. A crude estimate of the extension of the wave function is taking twice this diameter, thus ~ 9 nm. Yet, EMT neglects relaxation effect which can be important in very thin SiNWs and the dopant levels should be calculated directly.

The trend of the ionization energies vs diameter can be qualitatively obtained from DFT calculations (Durgun *et al.*, 2007a; Leão *et al.*, 2008). As we discussed in Section III.B.2, however, the local and semi-local approximations commonly used for the exchange-correlation energy severely underestimate the band gap and likewise the gap states and the related ionization energies. While the best suited approach for correct band gap calculations was the GW methodology (see Section III.B.2), it does not seem a viable solution for defective systems. Due to the need of simulating isolated impurities, computational supercells have to be large enough to allow neglecting the interaction of a defect with its periodic images. This implies a large number of atoms which is normally beyond the current computational capabilities of GW based codes.

Hybrid functionals –where a certain amount of exact Hartree-Fock exchange is mixed to conventional LDA/GGA functionals– provide accurate estimations of defect states in bulk Si (Deák *et al.*, 2005) and have also been used to calculate P donors in $\langle 110 \rangle$ and $\langle 111 \rangle$ SiNWs (Rurali *et al.*, 2009). As expected, these calculations yielded ionization energies that are deeper than the values obtained by DFT (Leão *et al.*, 2008), though the difference decreases for larger wires. Remarkably, P behaves as an EMT dopant down to diameters of 1.5 nm, its wave function highly localized, whereas it breaks down for wires of 1.0 nm diameter. For such small wires the wave function is qualitatively different: it significantly interacts with the surface and cannot be described as quasi-one dimensional confined EMT state.

3. Dielectric confinement

The estimation of the ionization energies of dopants in nanowires has also been tackled efficiently at the tight-binding level (Diarra *et al.*, 2008, 2007). We have already seen in Section III.B.2 that this approach can be complementary to the calculations at GW and hybrid-functional level (Niquet *et al.*, 2006). Its quantitative reliability could be questioned for ultra-thin wires (diameters smaller than 2 nm), because this model neglects relaxation effects, important for such wires, and relies on a parametrization obtained for bulk Si. On the other hand, it is the best alternative to deal with larger wires where confinement still produces sizeable effects. A remarkable feature of this approach is the flexibility with which the screening properties of the surrounding dielectric medium can be manipulated, allowing to study in detail the so-called *dielectric confinement*.

The Coulomb potential of an impurity gives rise to a bound state in the energy gap. In bulk Si this potential is strongly screened ($\epsilon_r = 11.3$), the Bohr radius is large, and the ionization energies amount to a few meV, so that the impurities are ionized at room temperature. The screening of a nucleus charge $+e$ leaves a total charge $+e/\epsilon$ at the impurity site, whereas the remaining charge $+e(1 - 1/\epsilon)$ is repelled at infinity. In a one dimensional system the screening properties are different. The charge $+e(1 - 1/\epsilon)$ must be repelled at the surface of the nanowire, leading to an extra term in the potential.

The physics of screening in one dimensional systems is straightforwardly incorporated in

the tight-binding Hamiltonian of Diarra *et al.* (2008, 2007):

$$H = H_0 + U_{imp} + \Sigma \quad (6)$$

where H_0 is the Hamiltonian of the undoped wire, $U_{imp} = \pm V(r, r_0)$ is the potential at r of an impurity at r_0 , and Σ is the self-energy potential, which accounts for the interaction between the carrier and the surface polarization charges induced by its own presence.

On the basis of this tight-binding model Diarra *et al.* (2007) showed that the ionization energies of typical donors are significantly deeper than in bulk, even for large wires ($d > 10$ nm) where the effects of quantum confinement are weak. This effect is due to the interaction between the electron and the surface polarization charge $+e(1 - 1/\epsilon)$. These results (i) indicate that dielectric confinement can be stronger than quantum confinement and that donor levels deepen more than how much the band gap broaden; (ii) the dielectric mismatch can be used to vary the ionization energies. In particular, a metallic or high-permittivity surrounding gate, present in realistic applications, is expected to reduce significantly the ionization energies. These predictions have been recently supported by the experimental results of Björk *et al.* (2009).

4. Metallic impurities

Although much of the attention has been devoted to dopants so far, metal impurities are becoming increasingly important for the reliability (Bailly *et al.*, 2008; Hannon *et al.*, 2006; den Hertog *et al.*, 2008; Oh *et al.*, 2008) and functionalization of SiNWs. Transition metals have attracted some interest because of their possible use in designing nanoscale dilute magnetic semiconductors (Durgun *et al.*, 2008; Giorgi *et al.*, 2008; Xu *et al.*, 2008). Room-temperature ferromagnetism in SiNWs has indeed been reported (Wu *et al.*, 2007), although the annealing conditions to stabilize the magnetization are very critical. The ferromagnetic coupling of Mn impurities is confirmed by electronic structure calculations. At variance with typical dopants these impurities do not segregate to the surface, at least in absence of surface DBs (Xu *et al.*, 2008), and they favor aggregation. This tendency has been reported to be important to stabilize the magnetism, because only when the Mn-Mn distance is below a certain cutoff ferromagnetic coupling is favored over antiferromagnetic coupling (Giorgi *et al.*, 2008).

It is interesting to observe that specific TM impurities can drive the nanowire to a half-metallic ground state. A half-metal is a system where one spin is metallic, whereas the other is insulating (de Groot *et al.*, 1983). Such systems have the greatest interest for spintronics applications, because naturally all the conduction electrons belong to the same spin and the spin polarization P is maximum ⁶. In the framework of a comprehensive analysis of surface adsorption of TM atoms in SiNWs, Durgun *et al.* (2007b) discovered that wires decorated with Co and Cr can be ferromagnetic half-metals. Upon adsorption of a Co or Cr atom at the surface, the spin degeneracy is lifted and, while the bands of majority spin continue being semiconducting, two minority spin bands made of hybridized TM-3d and Si-3p states cross the Fermi level driving the wire to half-metallicity. There is a sizeable charge transfer from the TM atom to the wire and the high values of the binding energies indicate strong bonds, which is important to prevent uncontrolled clustering that would be detrimental to the magnetic ordering. The half-metallicity is obtained for huge coverages (one impurity for primitive cell) typical of dilute magnetic semiconductors. As the coverage is reduced, the gap of the minority spins starts closing and the system is no longer half metallic ($P < 1$). However, the total spin polarization remains very high and close to its maximum permitted value.

5. Formation energy

The energetic cost of creating a defect is given by the *formation energy*. The formation energy is the main computational quantity describing the stability and energetics of a defect in a host material and it is essential to determine impurity equilibrium concentrations (Zhang and Northrup, 1991), solubilities (Van de Walle *et al.*, 1993) or diffusivities (Fahey *et al.*, 1989). In bulk systems the formation energy can be calculated according to the well established formalism of Zhang and Northrup (1991):

$$\Delta E^f = E_{tot}^D - \sum_i n_i \mu_i + q(\varepsilon_v + \mu_e), \quad (7)$$

where E_{tot}^D is the total energy of the defective system, n_i is the number of atoms belonging to species i with chemical potential μ_i , q is the net charge of the system, ε_v is the energy of

⁶ The spin polarization is normally defined as $P = (N^\uparrow - N^\downarrow)/(N^\uparrow + N^\downarrow)$, where $N^{\uparrow,\downarrow}$ are the densities of states at the Fermi level.

the top of the valence band of the clean host and μ_e is the chemical potential for electrons; the sum runs over all the species present in the system. However, the extension of Eq. 7 to one dimensional systems presents some subtleties. In particular, the chemical potential of the host species is ill-defined.

To see why, let us focus on the formation of a Si vacancy and let us play the movie of the wire growth: Si atoms start precipitating from the supersaturated Au-Si droplet and contribute to the nucleation of the wire; once in a while one Si atom does not *fill* the proper lattice site and a vacancy is formed. When calculating the formation energy one has to estimate the contribution to the total energy of this atom, the one that left the vacant site and was incorporated in the wire somewhere else. In bulk this is easy, because all the lattice sites are equivalent and then each atom contributes equally to the total energy. In a nanowire, on the other hand, this quantity is not well defined, because it depends where the misplaced atom is thought to end up, as the lattice sites are non-equivalent.

Rurali and Cartoixà (2009) have proposed a way to circumvent this problem that also deals with the passivating agents, if present. They showed that rewriting the equations for the formation of N defects at a time, being N the number of Si atoms in the primitive cell, leads to the definition of an *effective* chemical potential of the wire primitive cell. In this way, whenever the formation of a defect involves the addition/removal of an atom of the host species, e.g. vacancies, self-interstitials, substitutionals, it is transferred to/from the correct reservoir –the wire itself– and only easily computable quantities are involved.

A further problem arises when dealing with charged defects. In a periodic boundary condition formalism point charges result in an infinite electrostatic energy. This inconvenience can be obviated by using a compensating jellium background. The errors in the total energy are often corrected *a posteriori* by means of the Madelung energy (Makov and Payne, 1995), though other methods have been proposed. Again, this correction has to be properly generalized to be used in nanowires. In particular, in solids the Madelung correction is scaled by the value of the (isotropic) macroscopic dielectric constant of the host material. In nanowires, on the other hand, a dielectric tensor $\bar{\epsilon}$ will be needed for the correct description of the interaction between the different instances of the charged defect (Rurali and Cartoixà, 2009). Notice that the value of the dielectric tensor will depend on the ratio between the axial lattice parameter, the lateral vacuum buffer and the chosen values of the axial (Hamel *et al.*, 2008) and transverse components of the $\bar{\epsilon}$ tensor and therefore cannot be looked up in tables.

IV. TRANSPORT PROPERTIES

The study of electron and heat transport is one of the most rapidly growing research field in nanowires. The reason is twofold: on the one hand transport measurements often are the most direct and simplest way to test the theoretical predictions (Björk *et al.*, 2009; Chen *et al.*, 2008; Cui *et al.*, 2000; Li *et al.*, 2003; Sellier *et al.*, 2006; Yu *et al.*, 2000); on the other hand, the behavior can be much different from bulk Si and can be exploited for enhanced performances in applications, whereas other times it can be detrimental.

A. Electron transport

1. Surface roughness disorder

An important cause of the degradation of the electrical conductance in SiNW-based devices is the scattering occurring at the surface in presence of surface defects or surface roughness (Luisier *et al.*, 2007; Wang *et al.*, 2005). This is not unexpected, since we have seen that many properties are ruled by the large surface-to-volume ratio of SiNWs. Considering non-smooth surfaces has indeed a great importance, as SiNWs exhibiting either tapering (Kodambaka *et al.*, 2006; Wang *et al.*, 2006c; Wu *et al.*, 2008b) or fancier saw-tooth faceting (Ross *et al.*, 2005) are often reported.

The effects of surface roughness on electron transport have first been addressed by Svizhenko *et al.* (2007). They modeled the surface disorder adding with probability $1/2$ one monolayer at each facet of a given unit cell. Since the position of these surface bumps is uncorrelated, they obtained a *white-noise* roughness. The surface roughness originates strong irregularities in the density of states along the wire axis, which in turn causes reflection of carriers and a strong reduction of the conductance. When these effects sum up in very long wires the disorder quickly drives the transport into the Anderson localization regime (Anderson, 1958).

A complementary approach to the description of the surface roughness disorder has been followed by Persson *et al.* (2008) and Lherbier *et al.* (2008). They modeled the roughness as random fluctuations δr of the wire radius around its average value r_0 , through a Lorentzian autocorrelation function, obtaining a *correlated* disorder. They showed that the backscattering strongly depends on the nanowire orientation, the anisotropy coming from the differences

in the underlying band structure. In particular, electrons are less sensitive to surface roughness in $\langle 110 \rangle$ SiNWs, whereas holes are better transmitted in $\langle 111 \rangle$ SiNWs (Persson *et al.*, 2008). Also, as the disorder correlation length –roughly the length scale of the diameter fluctuations– increases, the lowest-lying states of the conduction band get trapped into the largest sections of the wire ⁷. The modified extent of the electron wave function affect many key quantities for transport, such as the mean free path and the localization length. Interestingly, the room temperature mobility of electrons and holes seems rather insensitive to short length scale fluctuations, as well to very long length scale fluctuations, a case in which the surface experienced by the carriers is locally smooth.

2. Single-impurity scattering

Besides surface disorder, the other main critical source of scattering is the presence of impurities. Surface scattering has a stronger impact on the transport in SiNWs than in bulk Si because of the much larger surface-to-volume ratio. The case of impurity scattering seems different, since it should solely depend on the impurity density and should affect in a similar way bulk Si and SiNWs. This is not the case, though. So, where is the catch?

With the reduction of the wire size below 10 nm, the impurity cross-sections become of the same order of the wire characteristic dimension and can result in total backscattering. In the semiclassical picture used to study transport in bulk materials impurities are point-like centers that scatter randomly the incoming carriers. This chaotic process slows down the carrier flow and results in a reduction of the conductance. The quantum picture in a thin one-dimensional medium is slightly different: impurities have to go through to a scattering potential that often extends throughout most of the wire cross-section and, following with the semiclassical analogy, the trajectories of the carriers are not simply deviated, but they can be entirely backscattered.

Impurity is a fairly generic denomination when referred to semiconductors. In fact, it refers to both undesired defects, by-products of an imperfect growth, and to dopants, which are purposely introduced to provide the material with tailor-made electric features. Clearly, this case is the most challenging: dopants increase the carrier density at device operation

⁷ A similar mechanism has been reported recently for selectively strained nanowires (Wu *et al.*, 2009).

temperature, but at the same time might induce a significant scattering which leads to a drop in the conductance. Fernández-Serra *et al.* (2006a) studied the resistance associated with a substitutional P impurity in the wire core, at the wire surface, and with a DB+impurity, a complex whose importance was discussed in a previous work of theirs (Fernández-Serra *et al.*, 2006b). Resonant backscattering –a strong reduction of the conductance in correspondence to impurity related bound states– is the main signature of substitutional impurities, though P in the core or at the surface yield different results. On the other hand, DB+impurity complexes are transparent to the incoming carriers and the transport is ballistic.

Therefore, donor impurities such as P either segregate to the surface where they are likely to form an electrically inactive complex with a DB or they stay in the wire core where they produce a strong backscattering, particularly at certain resonant energies. In both cases the current is reduced.

3. Multiple-impurity scattering

The calculations of Fernández-Serra and co-workers opened the field of dopant scattering in SiNWs, but they have two limitations: (i) they study the scattering properties of an individual impurity, while in realistic SiNWs the wire resistance results from multiple scattering events; (ii) impurities can be ionized, the typical situation for dopants, and the proper charge state must be taken into account in the conductance calculation.

The first of these two issues has been tackled by comparing the conductance evaluated directly in long wires, with a certain distribution of impurities, with the predictions that can be made on the basis of single-dopant calculations (Markussen *et al.*, 2007). This is a challenging task, because to make such a comparison on equal footing the long wire too has to be treated within a first-principle formalism, which involves an extraordinary computational load. This difficulty can be circumvented thanks to an ingenious method that allows constructing the Hamiltonian of the long wire assembling building blocks obtained from the single-dopant calculations (Markussen *et al.*, 2006). In this way the electronic structure problem has not to be solved directly in the long wire.

The surprising result is that the properties of long, realistic wires –such as mean free path, resistance vs length– can be *entirely* predicted from single-impurity conductances. So, the resistance of a wire with an arbitrary distribution of impurities is obtained by classically

adding the resistances of each individual scatterer according to Ohm’s law:

$$\langle R(L, E) \rangle = R_c(E) + \langle R_s(E) \rangle L/l \quad (8)$$

where $\langle R_s(E) \rangle$ is the average resistance that can be evaluated from the single-dopant calculations, $R_c(E)$ is the contact resistance, L is the length of the wire and l the average separation between dopants. Interestingly, a similar approach has been proposed also for phonon transport (Markussen *et al.*, 2009; Savić *et al.*, 2008).

This method allows easy comparisons of the conductance of wires with different distributions of defects. The case of P substitutionals, for instance, has been addressed by Markussen *et al.* (2008b), where a uniform radial distribution was compared to a mainly surface distribution, in accordance with the previously reported indications of P surface segregation (Fernández-Serra *et al.*, 2006b).

4. Charged impurity scattering

Addressing charged impurities poses well-known problems related to the use of periodic boundary conditions. Large supercells, out of the current capability of first-principles methods, are needed to allow the correct screening of the electrostatic potential of the impurity. The conductance depends more critically than other quantities on this incomplete screening.

Such systems have been dealt with within an approximate method that combine first-principle methods with finite element calculations of the electrostatic potential (Rurali *et al.*, 2008b). The idea is very simple. If a charged dopant is approximated with a point charge, its electrostatic potential can be obtained in a very cheap way with a finite element calculation. Far from the impurity this is a reasonable approximation –a P^+ impurity gives rise to essentially the same Coulomb potential of a As^+ impurity– and the agreement with a self-consistent electronic structure calculation is indeed very good. Close to the impurity, on the other hand, quantum electronic structure accounts properly for the different chemical nature of different impurities, a task not accomplished by a finite element model.

The part of the potential that converges slowly with the cell size is the long-range Coulomb potential. So, here comes the simple idea: the *local* potential around the impurity is calculated at the first-principle level in a large, but tractable computational cell. Then the long-range tails are calculated within a finite element model (which it is known to yield the

same result than a first-principle calculation). In this way one can in principle engineer arbitrary boundary conditions, as the long range part of the potential can be obtained at a negligible computational cost.

This approximated approach allows explicitly addressing the calculation of the conductance associated to impurities with different charge states and comparing majority carriers (electrons in a n -type wire, holes in p -type wire) vs minority carriers (electrons in a p -type wire, holes in n -type wire). The results are indeed utterly different and it is shown that in sufficiently thin wires minority carriers transmission is entirely suppressed (Rurali *et al.*, 2008b). What happens is that in the case of minority carriers the dopant constitutes an effective barrier in the potential landscape. When the energy of the electron is less than that of the barrier height, it must tunnel through the potential and the transmission is therefore exponentially suppressed.

B. Heat transport

Recently, there has been a lot of excitement around the thermal conductive properties of SiNWs. Surprisingly, this excitement stems from the *poor* thermal conductance of SiNWs. The reason is that the use of SiNWs as materials with enhanced thermoelectric properties has been demonstrated independently by two groups (Boukai *et al.*, 2008; Hochbaum *et al.*, 2008).

While in some devices one wants to get the heat away as efficiently as possible and a high thermal conductance is desirable, in thermoelectrics one wants a thermal conductance as small as possible (Cahill *et al.*, 2003). It has been suggested that at the nanoscale the thermoelectric efficiency could be increased with respect to bulk materials, since the electrical mobilities are expected to be higher, while the surface scattering of the phonons should decrease the lattice thermal conductance (Vo *et al.*, 2008). Recent experimental results have reported thermal conductivities of $\sim 1.6 \text{ W m}^{-1} \text{ K}^{-1}$, two orders of magnitude lower than the value for bulk Si ($150 \text{ W m}^{-1} \text{ K}^{-1}$ at room temperature).

Heat is transmitted by phonons, the vibrations of the crystal lattice. Calculating the phonon modes of a SiNW with a first-principles method is a demanding task and can be done only for the thinnest wires (Peelaers *et al.*, 2009). Fortunately, this is not too serious an inconvenience and the phonon band structure can be calculated with a great level of accuracy

within simple empirical interatomic potentials. It has been shown that phonon dispersions calculated with DFT and with the bond-order Tersoff potential (Tersoff, 1989) yield thermal conductances in excellent agreement (Markussen *et al.*, 2008a). It is indeed on the Stillinger-Weber potential that the first atomistic calculations of the thermal conductance of SiNWs were based on (Volz and Chen, 1999).

The decrease of the thermal conductance with the reduction of the diameter comes from the interplay of two factors: (a) phonon confinement, i.e. the change in the phonon spectra (Adu *et al.*, 2005) and (b) the increase of the inelastic phonon scattering at the surface. The dependence of the phonon dispersion on the wire size has been studied for $\langle 100 \rangle$ wires by Wang and Wang (2007), who showed that the thermal conductance decreases as the wire diameter is reduced. Ponomareva *et al.* (2007) obtained similar results for $\langle 111 \rangle$ wires, although the thermal conductance steeply increases again for diameters below 2 nm (Ponomareva *et al.*, 2007), a direct signature of phonon confinement. Namely, as the diameter is reduced the lowest frequency excited mode is severely affected by the confinement; this long wavelength mode dominates the low frequency spectrum and, carrying a larger amount of energy, determines the enhanced thermal conductance at small diameters⁸.

It should be bear in mind, however, that the effects of phonon confinement are normally studied in nanowires with an ideal structure, whereas in the recent reports of the enhanced thermoelectric figures of SiNWs surface corrugation seems to play an important role. Recently, Donadio and Galli (2009) showed that the computed thermal conductance strongly depends on the surface structure, whereas it can be insensitive to variations of the diameter in the size range investigated ($d < 4$ nm). Phonon confinement do not necessarily lead to low values of the thermal conductance, which in some cases can even increase as a function of size, due to the presence of long wavelength phonons with very long mean free paths, like shown by Ponomareva *et al.* (2007).

It is useful to consider these studies together, because of their complementary methodological approaches. Wang and Wang (2007) calculate the phonon dispersion with the usual procedure consisting in displacing each atom along $\pm x$, $\pm y$, and $\pm z$ to obtain the dynam-

⁸ A similar feature is also present in the $\langle 100 \rangle$ wires of Wang and Wang (2007), where for temperatures lower than 50 K the thermal conductance of a 1.54 nm wire is larger than the thermal conductance of a 4.61 nm wire. However, it is difficult to be more quantitative at this respect, due to the scale of the plots used in Wang and Wang (2007).

ical matrix by finite differences. Then they calculate the thermal conductance with non equilibrium Green's functions. In this way they rely on the harmonic approximation and thereby neglect any phonon-phonon scattering, an approach valid in the low to mid temperature limit. Similar calculations for thicker wires, $d > 35$ nm (Mingo, 2003; Mingo *et al.*, 2003), where phonon confinement effects are unimportant, yielded an excellent agreement with experimental results (Li *et al.*, 2003). Ponomareva *et al.* (2007) and Donadio and Galli (2009), on the other hand, calculate the thermal conductance within a molecular dynamics simulation from Fourier's law $J_z = -\sigma \partial T / \partial z$, where J_z is the heat flow along the wire axis z and $\partial T / \partial z$ is the thermal gradient (Schelling *et al.*, 2002). Within this scheme, one does not calculate explicitly the full phonon dispersion and anharmonic effects are automatically included in the simulation. The anharmonic forces are increasingly important at higher temperatures, since the atomic displacements get bigger. This means that phonon-phonon scattering becomes more and more important at higher temperatures and dominates over the effects of including more conducting channels. The drawback is that classical molecular dynamics is reliable only above the Debye temperature of the material (645 K for Si) where quantum effects in the ionic dynamics can be neglected and below it the results must be interpreted with some care.

It should not come as a surprise that the thermal conductance is also anisotropic, like many other important quantities that we have discussed throughout the paper. At low energy the phonon dispersion features four acoustic branches, one dilatational, one torsional, and two flexural modes (Thonhauser and Mahan, 2004). The torsional mode is related to rotational invariance around the wire axis, and it is similar for all the orientations. At higher energies, however, one can notice that the bands in $\langle 110 \rangle$ SiNWs have a larger slope, i.e. larger velocities, than the other orientations which feature mostly flat bands (see Fig. 12). Hence, at a given energy there are more bands in the $\langle 110 \rangle$ wire than in the $\langle 100 \rangle$ or $\langle 111 \rangle$ and consequently one expects a larger thermal conductance. Heat conductance is indeed strongly anisotropic. Up to ≈ 20 K, where the phonon dispersion is dominated by the acoustic modes, the thermal conductance is independent on the growth orientation, but then $\langle 110 \rangle$ SiNWs stand out, with an up to twofold increase in their conductance (Markussen *et al.*, 2008a).

V. CONCLUSIONS

In this paper we have reviewed the major advances in the theoretical study of the structural, electronic and transport properties of silicon nanowires. While the geometry and the electronic structure of nanowires are relatively well-understood, many open questions remain on the possibility of effectively dope ultra-thin nanowires and on many of the atomic scale mechanisms ruling electrical current and heat transport.

Silicon nanowires are rod-like system constructed around a single-crystalline core. The most important consequence of their monocrystallinity is that they grow along well-defined crystallographic orientations, and at sufficiently small diameters a strong anisotropy of most of their properties emerge: the band gap, the Young's modulus, the electrical conductance or the specific heat, just to name some, are different for wires grown along different orientations. The cross-sections are intimately related with the growth orientations –given a growth orientation only certain sets of bounding facets are allowed–, although their impact on the electronic properties of the wires seems limited, while other magnitudes such as the diameter or the surface-to-volume ratio have a greater influence. The band gap can be direct, opening the way to the use of Si in photonics, and can be tuned by varying the wire diameter, choosing the growth orientation or controlling the surface passivation. Extrinsic carrier conduction seems to be highly problematic and whether is feasible or not for ultra-thin nanowires is not clear yet. The reason is that dopant efficiency is bedeviled by multiple factors: surface segregation and clustering with consequent neutralization, deepening of the doping level due to dielectric and quantum confinement.

Many promising applications have already been demonstrated. Although the nanowires used in these applications are smaller than any device that can be fabricated with lithography based techniques, they are still larger than those studied theoretically, where quantum effects leave their clear signature. Whereas it is clear that nanowires will play an important role in the next generation of electronic devices, it is difficult to say if the use of such ultra-thin wires will be practical. Many of the properties of these extremely thin nanowires pose severe technological challenges, but at the same time represent extraordinary opportunities. Anisotropic band gaps that critically depend on the wire diameter are apparently incompatible with any standardized technological process, to give an example. However, once the growth orientation and wire thickness can be controlled with great precision this

would open up the possibility of band gap engineering, which would be extremely attractive for optoelectronics applications.

Joint efforts in theory and experiments hold the key to nanowires' future.

Acknowledgments

I am deeply indebted to Mads Brandbyge, Xavier Cartoixa, Ádám Gali, Nicolás Lorente, Anti-Pekka Jauho, Troels Markussen, Maurizia Palummo, and Jordi Suñé. I would like to thank all those who granted permission for using figures of their original works. Financial support by the Ramón y Cajal program of the Ministerio de Ciencia e Innovación and funding under Contract No. TEC2006-13731-C02-01 are greatly acknowledged.

References

- Adu, K. W., H. R. Gutierrez, U. J. Kim, G. U. Sumanasekera, and P. C. Eklund, 2005, *Nano Letters* **5**(3), 409.
- Akiyama, T., K. Nakamura, and T. Ito, 2006, *Phys. Rev. B* **74**(3), 033307.
- Anderson, P. W., 1958, *Phys. Rev.* **109**(5), 1492.
- Aradi, B., L. E. Ramos, P. Deák, T. Köhler, F. Bechstedt, R. Q. Zhang, and T. Frauenheim, 2007, *Phys. Rev. B* **76**(3), 035305.
- Aryasetiawan, F., and O. Gunnarsson, 1998, *Rep. Prog. Phys.* **61**(3), 237.
- Avramov, P. V., A. A. Kuzubov, A. S. Fedorov, P. B. Sorokin, F. N. Tomilin, and Y. Maeda, 2007, *Phys. Rev. B* **75**(20), 205427.
- Bailly, A., O. Renault, N. Barrett, L. F. Zagonel, P. Gentile, N. Pauc, F. Dhalluin, T. Baron, A. Chabli, J. C. Cezar, and N. B. Brookes, 2008, *Nano Lett.* **8**(11), 3709.
- Baumer, A., M. Stutzmann, M. S. Brandt, F. C. Au, and S. T. Lee, 2004, *Appl. Phys. Lett.* **85**(6), 943.
- Björk, M. T., B. J. Ohlsson, C. Thelander, A. I. Persson, K. Deppert, L. R. Wallenberg, and L. Samuelson, 2002, *Appl. Phys. Lett.* **81**(23), 4458.
- Björk, M. T., H. Schmid, J. Knoch, H. Riel, and W. Riess, 2009, *Nature Nanotech.* **4**(2), 103.
- Blase, X., and M.-V. Fernández-Serra, 2008, *Phys. Rev. Lett.* **100**(4), 046802.

- Boukai, A. I., Y. Bunimovich, J. Tahir-Kheli, J.-K. Yu, W. A. Goddard III, and J. R. Heath, 2008, *Nature* **451**(7175), 168.
- Bransden, B., and C. Joachain, 2000, *Quantum Mechanics* (Benjamin Cummings, Upper Saddle River, NJ).
- Bruneval, F., S. Botti, and L. Reining, 2005, *Phys. Rev. Lett.* **94**(21), 219701.
- Bruno, M., M. Palummo, A. Marini, R. Del Sole, V. Olevano, A. N. Kholod, and S. Ossicini, 2005, *Phys. Rev. B* **72**(15), 153310.
- Bruno, M., M. Palummo, A. Marini, R. Del Sole, and S. Ossicini, 2007a, *Phys. Rev. Lett.* **98**(3), 036807.
- Bruno, M., M. Palummo, S. Ossicini, and R. D. Sole, 2007b, *Surf. Sci.* **601**(13), 2707.
- Buda, F., J. Kohanoff, and M. Parrinello, 1992, *Phys. Rev. Lett.* **69**(8), 1272.
- Cahill, D. G., W. K. Ford, K. E. Goodson, G. D. Mahan, A. Majumdar, H. J. Maris, R. Merlin, and S. R. Phillpot, 2003, *J. Appl. Phys.* **93**(2), 793.
- Canham, L. T., 1990, *Appl. Phys. Lett.* **57**(10), 1046.
- Cao, J. X., X. G. Gong, and R. Q. Wu, 2007, *Phys. Rev. B* **75**(23), 233302.
- Cao, J. X., X. G. Gong, J. X. Zhong, and R. Q. Wu, 2006, *Phys. Rev. Lett.* **97**(13), 136105.
- Chadi, D. J., 1979, *Phys. Rev. Lett.* **43**(1), 43.
- Chan, T.-L., C. Ciobanu, F.-C. Chuang, N. Lu, C.-Z. Wang, and K.-M. Ho, 2006, *Nano Lett.* **6**(2), 277.
- Chan, T.-L., M. Tiago, E. Kaxiras, and J. Chelikowsky, 2008, *Nano Lett.* **8**(2), 596.
- Charlier, J.-C., X. Blase, and S. Roche, 2007, *Rev. Mod. Phys.* **79**(2), 677.
- Chen, R., A. I. Hochbaum, P. Murphy, J. Moore, P. Yang, and A. Majumdar, 2008, *Phys. Rev. Lett.* **101**(10), 105501.
- Chung, S.-W., J.-Y. Yu, and J. R. Heath, 2000, *Appl. Phys. Lett.* **76**(15), 2068.
- Coleman, N. R. B., M. A. Morris, T. R. Spalding, and J. D. Holmes, 2001a, *J. Am. Chem. Soc.* **123**(1), 187.
- Coleman, N. R. B., N. O'Sullivan, K. M. Ryan, T. A. Crowley, M. A. Morris, T. R. Spalding, D. C. Steytler, and J. D. Holmes, 2001b, *J. Am. Chem. Soc.* **123**(29), 7010.
- Colinge, J.-P., 2004, *Solid-State Electron.* **48**(6), 897 .
- Colombo, L., 2005, *Riv. Nuovo Cimento* **28**(10), 1.
- Cui, Y., X. Duan, J. Hu, and C. M. Lieber, 2000, *J. Phys. Chem. B* **104**(22), 5213.

Cui, Y., L. J. Lauhon, M. S. Gudiksen, J. Wang, and C. M. Lieber, 2001a, Appl. Phys. Lett. **78**(15), 2214.

Cui, Y., and C. M. Lieber, 2001, Science **291**(5505), 851.

Cui, Y., Q. Wei, H. Park, and C. M. Lieber, 2001b, Science **293**(5533), 1289.

Cui, Y., Z. Zhong, D. Wang, W. Wang, and C. Lieber, 2003, Nano Lett. **3**(2), 149.

Cullis, A. G., and L. T. Canham, 1991, Nature **353**(6342), 335.

De Padova, P., C. Quaresima, P. Perfetti, B. Olivieri, C. Leandri, B. Aufray, S. Vizzini, and G. Le Lay, 2008, Nano Lett. **8**(1), 271.

Deák, P., A. Gali, A. Sólyom, A. Buruzs, and T. Frauenheim, 2005, J. Phys.: Cond. Matter **17**(22), S2141.

Delley, B., and E. F. Steigmeier, 1995, Appl. Phys. Lett. **67**(16), 2370.

Diarra, M., C. Delerue, Y.-M. Niquet, and G. Allan, 2008, J. Appl. Phys. **103**(7), 073703.

Diarra, M., Y.-M. Niquet, C. Delerue, and G. Allan, 2007, Phys. Rev. B **75**(4), 045301.

Dick, K. A., K. Deppert, M. W. Larsson, T. Martensson, W. Seifert, and L. R. Wallenberg, 2004, Nature Mater. **3**(6), 380.

Donadio, D., and G. Galli, 2009, Phys. Rev. Lett. **102**(19), 195901.

Duan, X., Y. Huang, and C. M. Lieber, 2002, Nano Lett. **2**(5), 487.

Durgun, E., N. Akman, C. Ataca, and S. Ciraci, 2007a, Phys. Rev. B **76**(24), 245323.

Durgun, E., N. Akman, and S. Ciraci, 2008, Phys. Rev. B **78**(19), 195116.

Durgun, E., D. Cakir, N. Akman, and S. Ciraci, 2007b, Phys. Rev. Lett. **99**(25), 256806.

Fahey, P. M., P. B. Griffin, and J. D. Plummer, 1989, Rev. Mod. Phys. **61**(2), 289.

Fernández-Serra, M.-V., C. Adessi, and X. Blase, 2006a, Nano Lett. **6**(12), 2674.

Fernández-Serra, M. V., C. Adessi, and X. Blase, 2006b, Phys. Rev. Lett. **96**(16), 166805.

Ferry, D. K., 2008, Science **319**(5863), 579.

Giorgi, G., X. Cartoixà, A. Sgamellotti, and R. Rurali, 2008, Phys. Rev. B **78**(11), 115327.

Goldberger, J., A. I. Hochbaum, R. Fan, and P. Yang, 2006, Nano Lett. **6**(5), 973.

Goringe, C. M., D. R. Bowler, and E. Hernández, 1997, Rep. Prog. Phys. **60**(12), 1447.

de Groot, R. A., F. M. Mueller, P. G. vanEngen, and K. H. J. Buschow, 1983, Phys. Rev. Lett. **50**(25), 2024.

Gudiksen, M. S., L. J. Lauhon, J. Wang, D. C. Smith, and C. M. Lieber, 2002, Nature **415**(6872), 617.

- Guichard, A., D. Barsic, S. Sharma, T. Kamins, and M. Brongersma, 2006, *Nano Lett.* **6**(9), 2140.
- Hahm, J.-i., and C. M. Lieber, 2004, *Nano Lett.* **4**(1), 51.
- Hamel, S., A. J. Williamson, H. F. Wilson, F. Gygi, G. Galli, E. Ratner, and D. Wack, 2008, *Appl. Phys. Lett.* **92**(4), 043115.
- Hannon, J. B., S. Kodambaka, F. M. Ross, and R. M. Tromp, 2006, *Nature* **440**(7080), 69.
- He, R., and P. Yang, 2006, *Nat. Nanotechnol.* **1**, 42.
- den Hertog, M. I., J.-L. Rouviere, F. Dhalluin, P. J. Desré, P. Gentile, P. Ferret, F. Oehler, and T. Baron, 2008, *Nano Lett.* **8**(5), 1544.
- Hochbaum, A. I., R. Chen, R. D. Delgado, W. Liang, E. C. Garnett, M. Najarian, A. Majumdar, and P. Yang, 2008, *Nature* **451**(7175), 163.
- Hoffmann, S., I. Utke, B. Moser, J. Michler, S. H. Christiansen, V. Schmidt, S. Senz, P. Werner, U. Gösele, and C. Ballif, 2006, *Nano Lett.* **6**(4), 622.
- Hohenberg, P., and W. Kohn, 1964, *Phys. Rev.* **136**(3B), B864.
- Holmes, J. D., K. P. Johnston, R. C. Doty, and B. A. Korgel, 2000, *Science* **287**(5457), 1471.
- Hong, K.-H., J. Kim, S.-H. Lee, and J. K. Shin, 2008, *Nano Lett.* **8**(5), 1335.
- Hsin, C.-L., W. Mai, Y. Gu, Y. Gao, C.-T. Huang, Y. Liu, L.-J. Chen, and Z.-L. Wang, 2008, *Adv. Mater.* **20**(20), 3919.
- Hu, Y., J. Xiang, G. Liang, H. Yan, and C. M. Lieber, 2008, *Nano Lett.* **8**(3), 925.
- Huang, L., N. Lu, J.-A. Yan, M. Y. Chou, C.-Z. Wang, and K.-M. Ho, 2008, *J. Phys. Chem. C* **112**(40), 15680.
- Huang, Y., X. Duan, Y. Cui, L. J. Lauhon, K.-H. Kim, and C. M. Lieber, 2001, *Science* **294**(5545), 1313.
- Hybertsen, M. S., and M. Needels, 1993, *Phys. Rev. B* **48**(7), 4608.
- Iijima, S., 1991, *Nature* **354**(6348), 56.
- Iori, F., E. Degoli, M. Palummo, and S. Ossicini, 2008, *Superlattices Microstruct.* **44**(4–5), 337.
- Ismail-Beigi, S., and T. Arias, 1998, *Phys. Rev. B* **57**(19), 11923.
- Jones, R. O., and O. Gunnarsson, 1989, *Rev. Mod. Phys.* **61**(3), 689.
- Justo, J. F., M. Z. Bazant, E. Kaxiras, V. V. Bulatov, and S. Yip, 1998, *Phys. Rev. B* **58**(5), 2539.
- Justo, J. F., R. D. Menezes, and L. V. C. Assali, 2007, *Phys. Rev. B* **75**(4), 045303.
- Kaczmariski, M., O. N. Bedoya-Martínez, and E. R. Hernández, 2005, *Phys. Rev. Lett.* **94**(9), 095701.

- Kagimura, R., R. W. Nunes, and H. Chacham, 2005, Phys. Rev. Lett. **95**(11), 115502.
- Kempa, T. J., B. Tian, D. R. Kim, J. Hu, X. Zheng, and C. M. Lieber, 2008, Nano Lett. **8**(10), 3456.
- Kizuka, T., Y. Takatani, K. Asaka, and R. Yoshizaki, 2005, Phys. Rev. B **72**(3), 035333.
- Kobayashi, K., 2004, Phys. Rev. B **69**(11), 115338.
- Kodambaka, S., J. Tersoff, M. C. Reuter, and F. M. Ross, 2006, Phys. Rev. Lett. **96**(9), 096105.
- Kohn, W., and L. J. Sham, 1965, Phys. Rev. **140**(4A), A1133.
- Kumar, V. (ed.), 2007, *Nanosilicon* (Elsevier, Amsterdam, The Netherlands).
- Leão, C. R., A. Fazzio, and A. J. R. da Silva, 2007, Nano Lett. **7**(5), 1172.
- Leão, C. R., A. Fazzio, and A. J. R. da Silva, 2008, Nano Lett. **8**(7), 1866.
- Lee, B., and R. E. Rudd, 2007a, Phys. Rev. B **75**(19), 195328.
- Lee, B., and R. E. Rudd, 2007b, Phys. Rev. B **75**(4), 041305(R).
- Lee, J.-H., G. A. Galli, and J. C. Grossman, 2008, Nano Lett. **8**(11), 3750.
- Lehmann, V., and U. Gösele, 1991, Appl. Phys. Lett. **58**(8), 856.
- Leu, P. W., B. Shan, and K. Cho, 2006, Phys. Rev. B **73**(19), 195320.
- Leu, P. W., A. Svizhenko, and K. Cho, 2008, Phys. Rev. B **77**(23), 235305.
- Lherbier, A., M. P. Persson, Y.-M. Niquet, F. Triozon, and S. Roche, 2008, Phys. Rev. B **77**(8), 085301.
- Li, B., A. F. Slachmuylders, B. Partoens, W. Magnus, and F. M. Peeters, 2008, Phys. Rev. B **77**(11), 115335.
- Li, B.-x., P.-l. Cao, R. Q. Zhang, and S. T. Lee, 2002, Phys. Rev. B **65**(12), 125305.
- Li, D., Y. Wu, P. Kim, L. Shi, P. Yang, and A. Majumdar, 2003, Appl. Phys. Lett. **83**(14), 2934.
- Li, Y., F. Qian, J. Xiang, and C. M. Lieber, 2006, Materials Today **9**(10), 18.
- Lu, A. J., R. Q. Zhang, and S. T. Lee, 2008a, Appl. Phys. Lett. **92**(20), 203109.
- Lu, W., and C. M. Lieber, 2006, J. Phys. D: Appl. Phys. **39**(21), R387.
- Lu, W., P. Xie, and C. Lieber, 2008b, Electron Devices, IEEE Transactions on **55**(11), 2859.
- Lugstein, A., M. Steinmair, Y. J. Hyun, G. Hauer, P. Pongratz, and E. Bertagnolli, 2008, Nano Lett. **8**(8), 2310.
- Luisier, M., A. Schenk, and W. Fichtner, 2007, Appl. Phys. Lett. **90**(10), 102103.
- Ma, D. D. D., C. S. Lee, F. C. K. Au, S. Y. Tong, and S. T. Lee, 2003, Science **299**(5614), 1874.
- Ma, L., J. Wang, J. Zhao, and G. Wang, 2008, Chem. Phys. Lett. **452**(1-3), 183.

- Makov, G., and M. C. Payne, 1995, Phys. Rev. B **51**(7), 4014.
- Marks, L. D., 1994, Rep. Prog. Phys. **57**, 603.
- Markussen, T., A.-P. Jauho, and M. Brandbyge, 2008a, Nano Lett. **8**(11), 3771.
- Markussen, T., A.-P. Jauho, and M. Brandbyge, 2009, Phys. Rev. B **79**(3), 035415.
- Markussen, T., R. Rurali, M. Brandbyge, and A.-P. Jauho, 2006, Phys. Rev. B **74**(24), 245313.
- Markussen, T., R. Rurali, A.-P. Jauho, and M. Brandbyge, 2007, Phys. Rev. Lett. **99**(7), 076803.
- Markussen, T., R. Rurali, A.-P. Jauho, and M. Brandbyge, 2008b, J. Comp. Electr. **7**(3), 324.
- Marsen, B., and K. Sattler, 1999, Phys. Rev. B **60**(16), 11593.
- Martin, R. M., 2004, *Electronic Structure: Basic Theory and Practical Methods* (Cambridge University Press, Cambridge, UK).
- Menon, M., and E. Richter, 1999, Phys. Rev. Lett. **83**(4), 792.
- Menon, M., D. Srivastava, I. Ponomareva, and L. A. Chernozatonskii, 2004, Phys. Rev. B **70**(12), 125313.
- Mingo, N., 2003, Phys. Rev. B **68**(11), 113308.
- Mingo, N., L. Yang, D. Li, and A. Majumdar, 2003, Nano Lett. **3**(12), 1713.
- Moon, C.-Y., W.-J. Lee, and K. J. Chang, 2008, Nano Lett. **8**(10), 3086.
- Moore, G., 1965, Electronics Magazine **38**(8).
- Morales, A. M., and C. M. Lieber, 1998, Science **279**(5348), 208.
- Muller, R. S., and T. I. Kamins, 1986, *Device Electronics for Integrated Circuits* (John Wiley & Sons, Hoboken, NJ).
- Neto, A. H. C., F. Guinea, N. M. R. Peres, K. S. Novoselov, and A. K. Geim, 2009, Rev. Mod. Phys. **81**(1), 109.
- Ng, H. T., J. Han, T. Yamada, P. Nguyen, Y. P. Chen, and M. Meyyappan, 2004, Nano Letters **4**(7), 1247.
- Ng, M.-F., L. Zhou, S.-W. Yang, L. Y. Sim, V. B. C. Tan, and P. Wu, 2007, Phys. Rev. B **76**(15), 155435.
- Niquet, Y. M., A. Lherbier, N. H. Quang, M. V. Fernández-Serra, X. Blase, and C. Delerue, 2006, Phys. Rev. B **73**(16), 165319.
- Nolan, M., S. O'Callaghan, G. Fagas, J. Greer, and T. Frauenheim, 2007, Nano Lett. **7**(1), 34.
- Northrup, J. E., 1991, Phys. Rev. B **44**(3), 1419.
- Oberlin, A., M. Endo, and T. Koyama, 1976, J. of Crystal Growth **32**, 335.

- Oh, S. H., K. v. Benthem, S. I. Molina, A. Y. Borisevich, W. Luo, P. Werner, N. D. Zakharov, D. Kumar, S. T. Pantelides, and S. J. Pennycook, 2008, *Nano Lett.* **8**(4), 1016.
- Ohno, T., K. Shiraishi, and T. Ogawa, 1992, *Phys. Rev. Lett.* **69**(16), 2400.
- Ossicini, S., C. M. Bertoni, M. Biagini, A. Lugli, G. Roma, and O. Bisi, 1997, *Thin Solid Films* **297**(1-2), 154 .
- Pandey, K. C., 1981, *Phys. Rev. Lett.* **47**(26), 1913.
- Patolsky, F., and C. M. Lieber, 2005, *Materials Today* **8**(4), 20.
- Pauzauskie, P. J., and P. Yang, 2006, *Mat. Tod.* **9**(10), 36.
- Payne, M. C., M. P. Teter, D. C. Allan, T. A. Arias, and J. D. Joannopoulos, 1992, *Rev. Mod. Phys.* **64**(4), 1045.
- Peelaers, H., B. Partoens, and F. Peeters, 2006, *Nano Lett.* **6**(12), 2781.
- Peelaers, H., B. Partoens, and F. M. Peeters, 2009, *Nano Lett.* **9**(1), 107.
- Pereira, R. N., A. R. Stegner, T. Andlauer, K. Klein, H. Wiggers, M. S. Brandt, and M. Stutzmann, 2009, *Phys. Rev. B* **79**(16), 161304(R).
- Perepichka, D. F., and F. Rosei, 2006, *Small* **2**(1), 22.
- Persson, M. P., A. Lherbier, Y.-M. Niquet, F. Triozon, and S. Roche, 2008, *Nano Lett.* **8**(12), 4146.
- Ponomareva, I., M. Menon, E. Richter, and A. N. Andriotis, 2006, *Phys. Rev. B* **74**(12), 125311.
- Ponomareva, I., M. Menon, D. Srivastava, and A. N. Andriotis, 2005, *Phys. Rev. Lett.* **95**(26), 265502.
- Ponomareva, I., D. Srivastava, and M. Menon, 2007, *Nano Lett.* **7**(5), 1155.
- Radushkevich, L., and V. Lukyanovich, 1952, *Zurn. Fisic. Chim.* **26**, 88.
- Read, A. J., R. J. Needs, K. J. Nash, L. T. Canham, P. D. J. Calcott, and A. Qteish, 1992, *Phys. Rev. Lett.* **69**(8), 1232.
- Ross, F. M., J. Tersoff, and M. C. Reuter, 2005, *Phys. Rev. Lett.* **95**(14), 146104.
- Rowe, A. C. H., 2008, *Nature Nanotech.* **3**(6), 311.
- Rurali, R., 2005, *Phys. Rev. B* **71**(20), 205405.
- Rurali, R., B. Aradi, T. Frauenheim, and A. Gali, 2007a, *Phys. Rev. B* **76**(11), 113303.
- Rurali, R., B. Aradi, T. Frauenheim, and A. Gali, 2009, *Phys. Rev. B* **79**(7), 115303.
- Rurali, R., and X. Cartoixà, 2009, *Nano Lett.* **0**(0).
- Rurali, R., X. Cartoixà, and D. S. Galvão, 2008a, *Phys. Rev. B* **77**(7), 073403.
- Rurali, R., and N. Lorente, 2005a, *Phys. Rev. Lett.* **94**(2), 026805.

- Rurali, R., and N. Lorente, 2005b, *Nanotechnology* **16**, S250.
- Rurali, R., T. Markussen, J. S. né, M. Brandbyge, and A.-P. Jauho, 2008b, *Nano Lett.* **8**(9), 2825.
- Rurali, R., A. Poissier, and N. Lorente, 2006, *Phys. Rev. B* **74**(16), 165324.
- Rurali, R., J. Suñe, and X. Cartoixà, 2007b, *Appl. Phys. Lett.* **90**(8), 083118.
- Saitta, A. M., F. Buda, G. Fiumara, and P. V. Giaquinta, 1996, *Phys. Rev. B* **53**(3), 1446.
- San Paulo, A., N. Arellano, J. A. Plaza, R. He, C. Carraro, R. Maboudian, R. T. Howe, J. Bokor, and P. Yang, 2007, *Nano Lett.* **7**(4), 1100.
- Sanders, G. D., and Y.-C. Chang, 1992, *Phys. Rev. B* **45**(16), 9202.
- Savić, I., N. Mingo, and D. A. Stewart, 2008, *Phys. Rev. Lett.* **101**(16), 165502.
- Scheel, H., S. Reich, and C. Thomsen, 2005, *phys. stat. sol. (b)* **242**(12), 2474.
- Schelling, P. K., S. R. Phillpot, and P. Keblinski, 2002, *Phys. Rev. B* **65**(14), 144306.
- Schmidt, V., S. Senz, and U. Gösele, 2005, *Nano Lett.* **5**(5), 931.
- Schwarz, K. W., and J. Tersoff, 2009, *Phys. Rev. Lett.* **102**(20), 206101.
- Sellier, H., G. P. Lansbergen, J. Caro, S. Rogge, N. Collaert, I. Ferain, M. Jurczak, and S. Biesemans, 2006, *Phys. Rev. Lett.* **97**(20), 206805.
- Sen, P., O. Gülseren, T. Yildirim, I. P. Batra, and S. Ciraci, 2002, *Phys. Rev. B* **65**(23), 235433.
- Sha, J., J. Niu, X. Ma, J. Xu, X. Zhang, Q. Yang, and D. Yang, 2002, *Adv. Mater.* **14**(17), 1219.
- Singh, A., V. Kumar, R. Note, and Y. Kawazoe, 2005, *Nano Lett.* **5**(11), 2302.
- Singh, A., V. Kumar, R. Note, and Y. Kawazoe, 2006, *Nano Lett.* **6**(5), 920.
- Slater, J. C., and G. F. Koster, 1954, *Phys. Rev.* **94**(6), 1498.
- Sorokin, P. B., P. V. Avramov, A. G. Kvashnin, D. G. Kvashnin, S. G. Ovchinnikov, and A. S. Fedorov, 2008, *Phys. Rev. B* **77**(23), 235417.
- Stillinger, F. H., and T. A. Weber, 1985, *Phys. Rev. B* **31**(8), 5262.
- Svizhenko, A., P. W. Leu, and K. Cho, 2007, *Phys. Rev. B* **75**(12), 125417.
- Tabib-Azar, M., M. Nassirou, R. Wang, S. Sharma, T. I. Kamins, M. S. Islam, and R. S. Williams, 2005, *Appl. Phys. Lett.* **87**(11), 113102.
- Takeguchi, M., M. Tanaka, H. Yasuda, and K. Furuya, 2001, *Surf. Sci.* **493**(1-3), 414 .
- Teo, B., X. Sun, T. Hung, X. Meng, N. Wong, and S. Lee, 2003, *Nano Lett.* **3**(12), 1735.
- Tersoff, J., 1989, *Phys. Rev. B* **39**(8), 5566.
- Thelander, C., P. Agarwal, S. Brongersma, J. Eymery, L. Feiner, A. Forchel, M. Scheffler, W. Riess, B. Ohlsson, U. Gösele, and L. Samuelson, 2006, *Mat. Tod.* **9**(10), 28.

Thelander, C., T. M. rtensson, M. T. Björk, B. J. Ohlsson, M. W. Larsson, L. R. Wallenberg, and L. Samuelson, 2003, Appl. Phys. Lett. **83**(10), 2052.

Thonhauser, T., and G. D. Mahan, 2004, Phys. Rev. B **69**(7), 075213.

Tian, B., T. J. Kempa, and C. M. Lieber, 2009, Chem. Soc. Rev. **38**, 16.

Tian, B., X. Zheng, T. J. Kempa, Y. Fang, N. Yu, G. Yu, J. Huang, and C. M. Lieber, 2007, Nature **449**(7164), 885.

Vo, T., A. J. Williamson, and G. Galli, 2006, Phys. Rev. B **74**(4), 045116.

Vo, T. T., A. J. Williamson, V. Lordi, and G. Galli, 2008, Nano Lett. **8**(4), 1111.

Volz, S. G., and G. Chen, 1999, Appl. Phys. Lett. **75**(14), 2056.

Wagner, R. S., and W. C. Ellis, 1964, Appl. Phys. Lett. **4**(5), 89.

Van de Walle, C. G., D. B. Laks, G. F. Neumark, and S. T. Pantelides, 1993, Phys. Rev. B **47**(15), 9425.

Wang, C., M. Hirano, and H. Hosono, 2006a, Nano Lett. **6**(7), 1552.

Wang, D., B. A. Sheriff, and J. R. Heath, 2006b, Nano Letters **6**(6), 1096.

Wang, J., E. Polizzi, A. Ghosh, S. Datta, and M. Lundstrom, 2005, Appl. Phys. Lett. **87**(4), 043101.

Wang, J., and J.-S. Wang, 2007, Appl. Phys. Lett. **90**(24), 241908.

Wang, N., Y. Cai, and R. Zhang, 2008, Mater. Sci. Eng. R **60**(1–6), 1.

Wang, N., Y. H. Tang, Y. F. Zhang, C. S. Lee, and S. T. Lee, 1998, Phys. Rev. B **58**(24), R16024.

Wang, S.-W., L. M. Falicov, and A. W. Searcy, 1984, Surf. Sci. **143**(2-3), 609.

Wang, Y., V. Schmidt, S. Senz, and U. Gösele, 2006c, Nature Nanotech. **1**(3), 186.

Westwater, J., D. P. Gosain, S. Tomiya, S. Usui, and H. Ruda, 1997, J. Vac. Sci. Technol. B **15**(3), 554.

Williamson, A. J., J. C. Grossman, R. Q. Hood, A. Puzder, and G. Galli, 2002, Phys. Rev. Lett. **89**(19), 196803.

Wu, H. W., C. J. Tsai, and L. J. Chen, 2007, Appl. Phys. Lett. **90**(4), 043121.

Wu, X., J. S. Kulkarni, G. Collins, N. Petkov, D. Almecija, J. J. Boland, D. Erts, and J. D. Holmes, 2008a, Chem. Mater. **20**(19), 5954.

Wu, Y., Y. Cui, L. Huynh, C. Barrelet, D. Bell, and C. Lieber, 2004, Nano Lett. **4**(3), 433.

Wu, Z., J. B. Neaton, and J. C. Grossman, 2008b, Phys. Rev. Lett. **100**(24), 246804.

Wu, Z., J. B. Neaton, and J. C. Grossman, 2009, Nano Lett., in press .

- Xia, J.-B., and Y.-C. Chang, 1993, Phys. Rev. B **48**(8), 5179.
- Xia, J.-B., and K. W. Cheah, 1997, Phys. Rev. B **55**(23), 15688.
- Xia, Y., P. Yang, Y. Sun, Y. Wu, B. Mayers, B. Gates, Y. Yin, F. Kim, and H. Yan, 2003, Adv. Mat. **15**(5), 353.
- Xu, Q., J. Li, S.-S. Li, and J.-B. Xia, 2008, J. Appl. Phys. **104**(8), 084307.
- Yan, J.-A., L. Yang, and M. Y. Chou, 2007, Phys. Rev. B **76**(11), 115319.
- Yao, D., G. Zhang, and B. Li, 2008, Nano Lett. **8**(12), 4557.
- Yeh, C.-Y., S. B. Zhang, and A. Zunger, 1994, Phys. Rev. B **50**(19), 14405.
- Yu, J.-Y., S.-W. Chung, and J. R. Heath, 2000, J. Phys. Chem. B **104**(50), 11864.
- Zdetsis, A. D., E. N. Koukaras, and C. S. Garoufalidis, 2007, Appl. Phys. Lett. **91**(20), 203112.
- Zhang, R. Q., Y. Lifshitz, D. D. D. Ma, Y. L. Zhao, T. Frauenheim, S. T. Lee, and S. Y. Tong, 2005, J. Chem. Phys. **123**(14), 144703.
- Zhang, S. B., and J. E. Northrup, 1991, Phys. Rev. Lett. **67**(17), 2339.
- Zhang, Y. F., L. S. Liao, W. H. Chan, S. T. Lee, R. Sammynaiken, and T. K. Sham, 2000, Phys. Rev. B **61**(12), 8298.
- Zhao, X., C. M. Wei, L. Yang, and M. Y. Chou, 2004, Phys. Rev. Lett. **92**(23), 236805.
- Zhao, Y., and B. I. Yakobson, 2003, Phys. Rev. Lett. **91**(3), 035501.
- Zhdanov, V. P., and B. Kasemo, 1998, Phys. Rev. Lett. **81**(12), 2482.
- Zheng, G., W. Lu, S. Jin, and C. M. Lieber, 2004, Adv. Mat. **16**(21), 1890.
- Zheng, K., X. Han, L. Wang, Y. Zhang, Y. Yue, Y. Qin, X. Zhang, and Z. Zhang, 2009, Nano Lett., in press .
- Zhong, J., and G. M. Stocks, 2006, Nano Lett. **6**(1), 128.
- Zhong, Z., Y. Fang, W. Lu, and C. M. Lieber, 2005, Nano Lett. **5**(6), 1143.
- Zhong, Z., D. Wang, Y. Cui, M. W. Bockrath, and C. M. Lieber, 2003, Science **302**(5649), 1377.

Figures

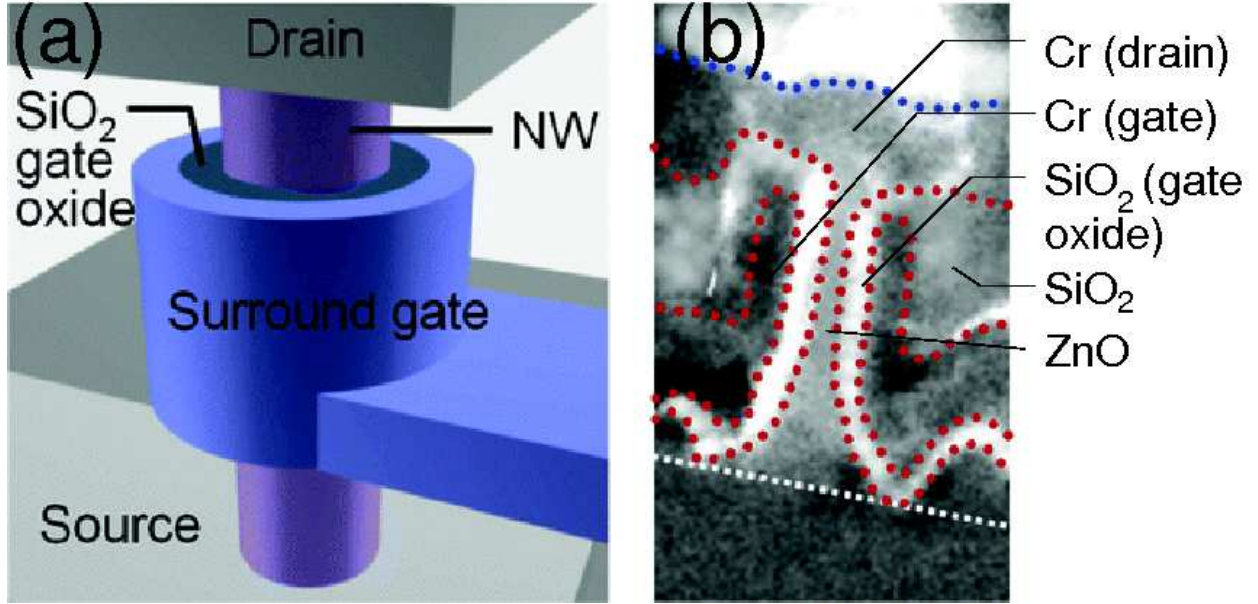


FIG. 1 (Color online) (a) Cartoon and (b) experimental realization of a ZnO nanowire-based field-effect transistor with an *all-around* (or surrounding) gate. The channel length is 200 nm. From Ng *et al.* (2004).

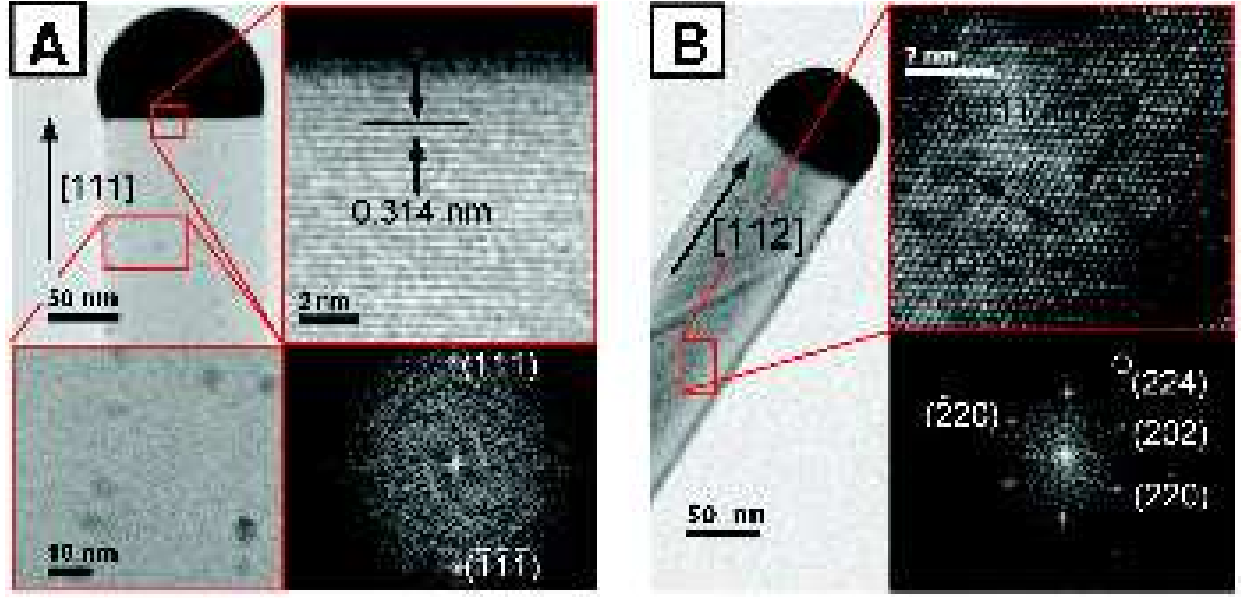


FIG. 2 (Color online) Transmission electron microscopy (TEM) image of a single crystalline SiNW grown along (a) the $\langle 111 \rangle$ and (b) the $\langle 112 \rangle$ axis. The high resolution TEM micrograph of the crystalline core shows clearly the Si(111) and Si(224) planes, respectively, together with the Fourier transform of the image. In case of the $\langle 111 \rangle$ SiNW a magnified view of the sidewalls of the wire show the presence of Au-Si particles about 7 nm in size. From Lugstein *et al.* (2008).

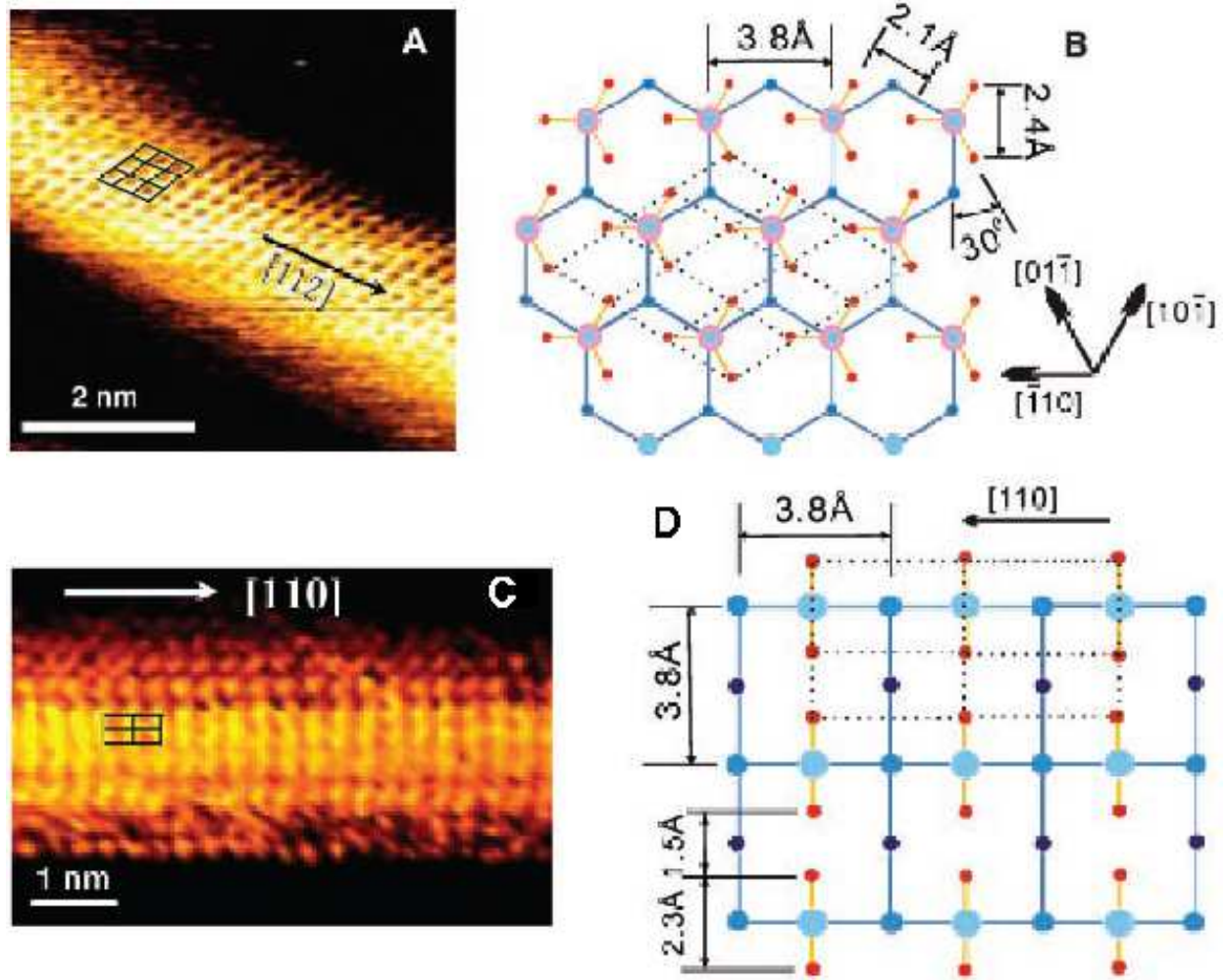


FIG. 3 (Color online) (a) Constant-current scanning tunneling microscope (STM) image of the $\{111\}$ facet of a SiNW grown along the $\langle 112 \rangle$ direction; (b) Schematic view of SiH_3 on $\text{Si}(111)$ viewed along the $\langle 111 \rangle$ direction; (c) Constant-current STM image of the $\{100\}$ facet of a SiNW grown along the $\langle 110 \rangle$ direction; (d) Schematic view of the dihydride phase on $\text{Si}(001)$. Red and large blue circles represent the H atoms and Si atoms, respectively. Small blue circles correspond to Si atoms on the underlying layers. The $\langle 112 \rangle$ wire in panel (a), with a diameter of 1.3 nm, is the thinnest SiNW reported to date. Adapted from Ma *et al.* (2003). Reprinted with permission from AAAS.

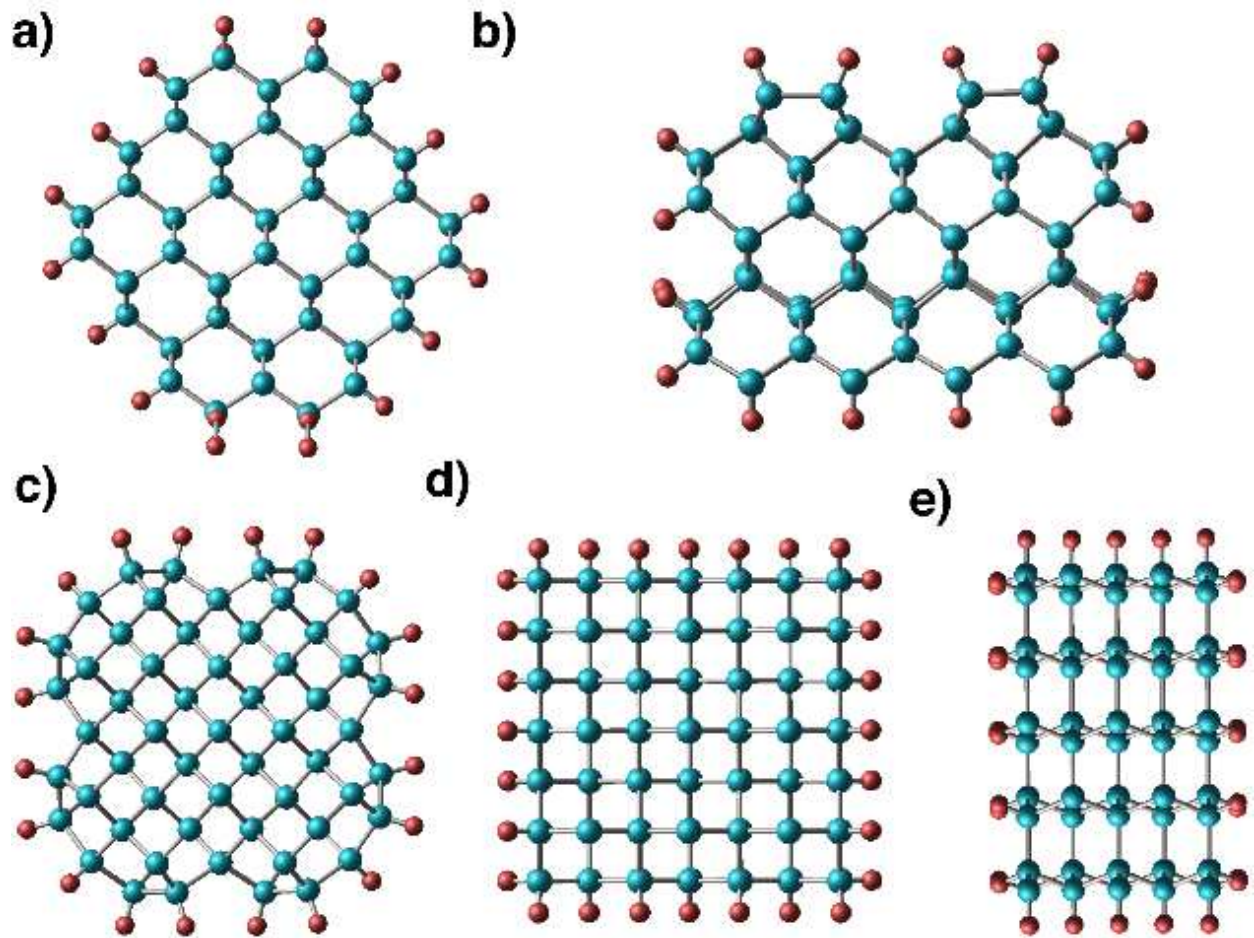


FIG. 4 (Color online) Optimized structures of possible cross-sections of H-passivated SiNWs grown along (a,b) the $\langle 110 \rangle$ (c,d) the $\langle 100 \rangle$ and (e) $\langle 112 \rangle$ orientation. Adapted from Singh *et al.* (2006).

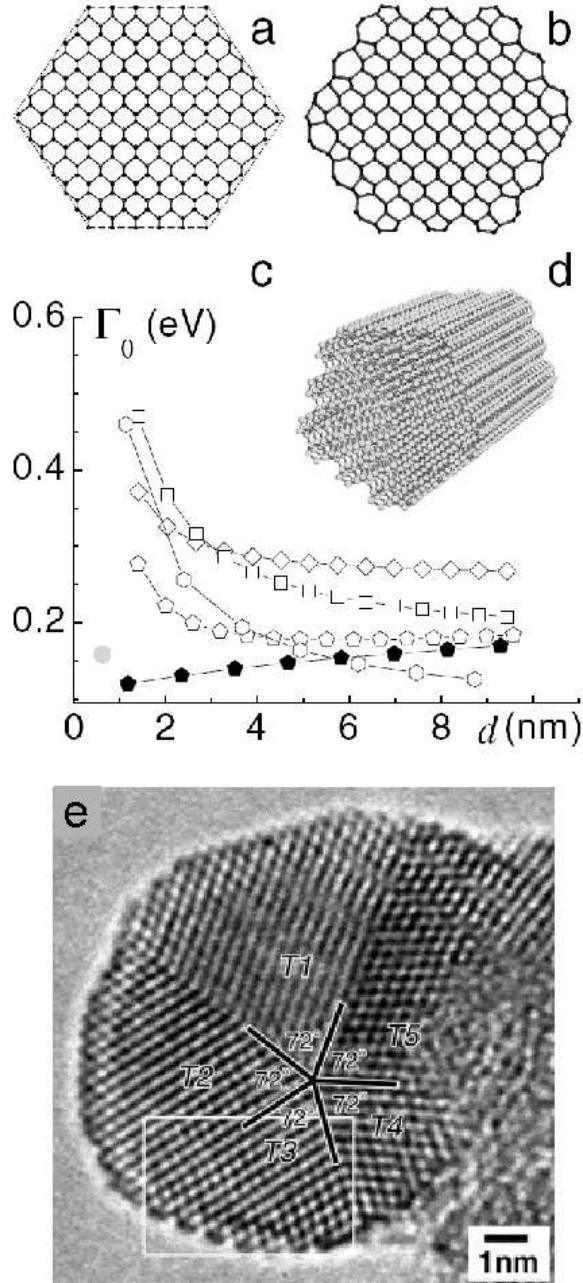


FIG. 5 Hexagonal $\langle 110 \rangle$ wire with four $\{111\}$ and two $\{100\}$ (a) unreconstructed and (b) reconstructed facets. (c) Energy of different types of wires (see Zhao and Yakobson (2003)) as a function of their diameter d . The most stable structure for $d < 6$ nm is [solid pentagons in panel (c)] is shown in panel (d). Panel (d) shows a high resolution TEM image of a pentagonal nanowire grown by Takeguchi *et al.* (2001). Adapted from Zhao and Yakobson (2003) and Takeguchi *et al.* (2001).

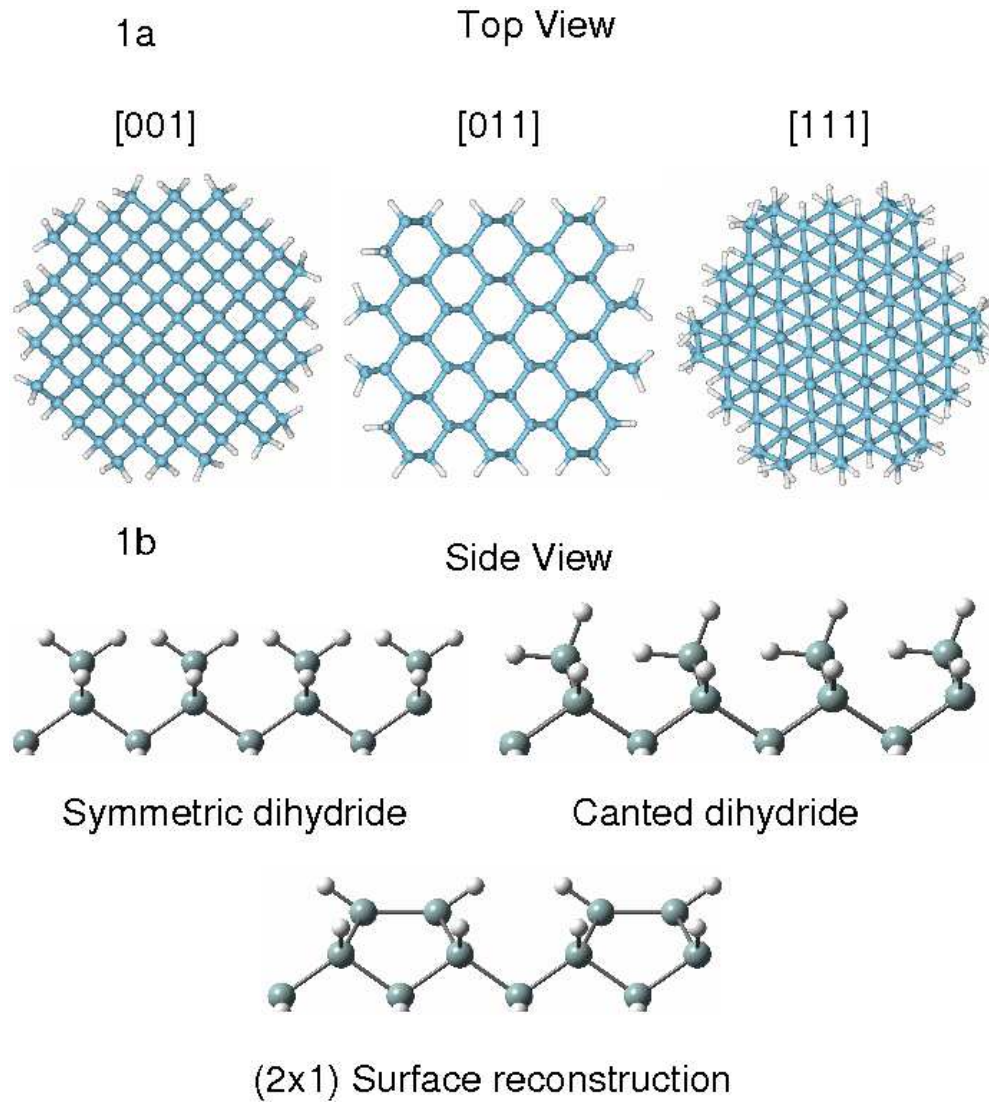


FIG. 6 (Color online) (a) Cross-section view of 3 nm SiNWs grown along three different directions $\langle 100 \rangle$, $\langle 110 \rangle$, and $\langle 111 \rangle$. (b) Side view of three different surface structures; in the last configuration the surface first reconstructs and then is passivated. From Vo *et al.* (2006).

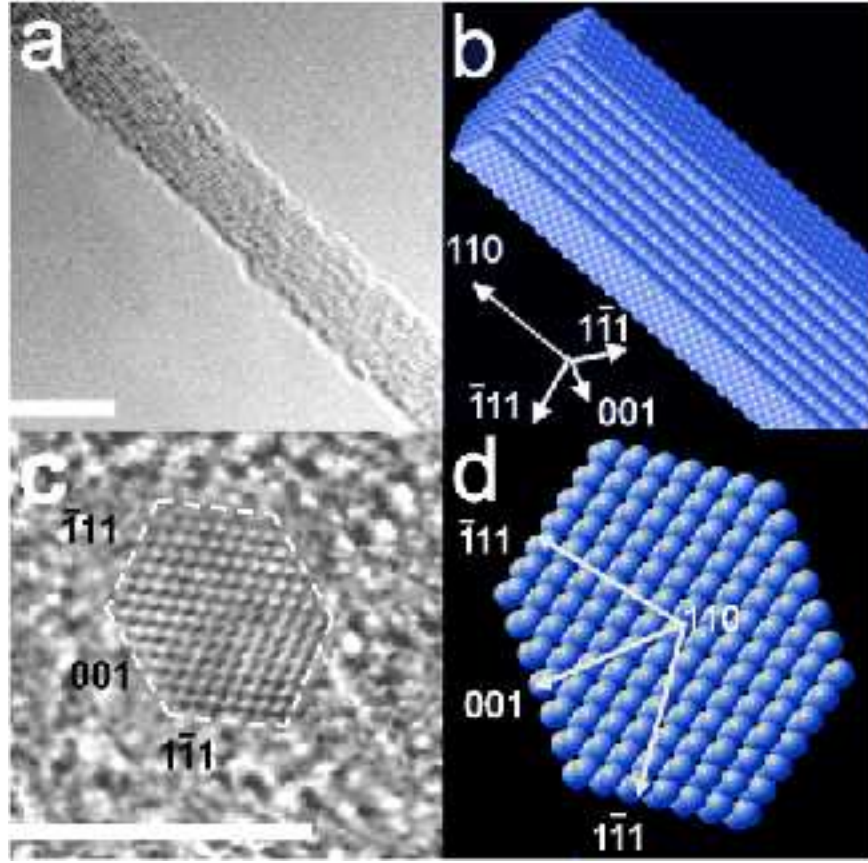


FIG. 7 (Color online) (a) TEM images of 3.8 nm SiNWs grown along the $\langle 110 \rangle$ direction, (c) high resolution TEM cross-sectional image, and equilibrium shapes for the (b) NW and the (d) NW cross-sections predicted by Wulff construction. The scale bars are 5 nm. From Wu *et al.* (2004).

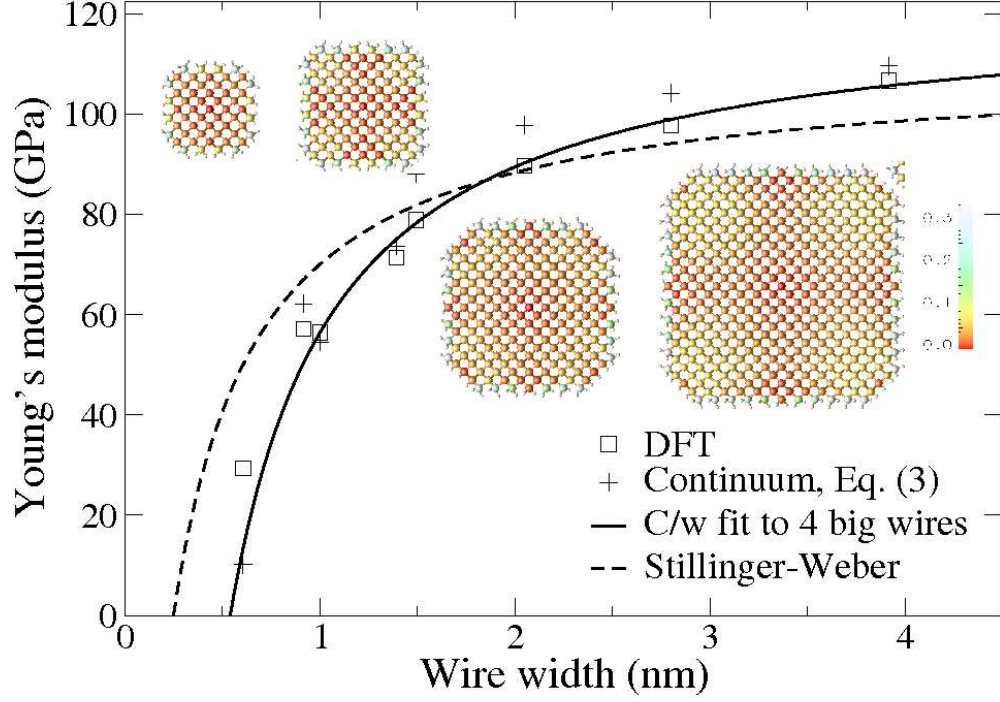


FIG. 8 (Color online) Young's modulus calculated within DFT as a function of wire size. For comparison values of continuum formula are also plotted. The solid curve $E = E_{bulk}^{DFT} - C/w$, where w is the width of the wire and $C = 66.11$ GPa/nm, is the best fit to a pure surface area to volume size dependence. (Insets) Cross sections of some of the SiNWs studied, where each Si atom is colored corresponding to its transverse relaxation in Å. The widths of wires are (a) 1.49, (b) 2.05, (c) 2.80, and (d) 3.92 nm. Adapted from Lee and Rudd (2007b).

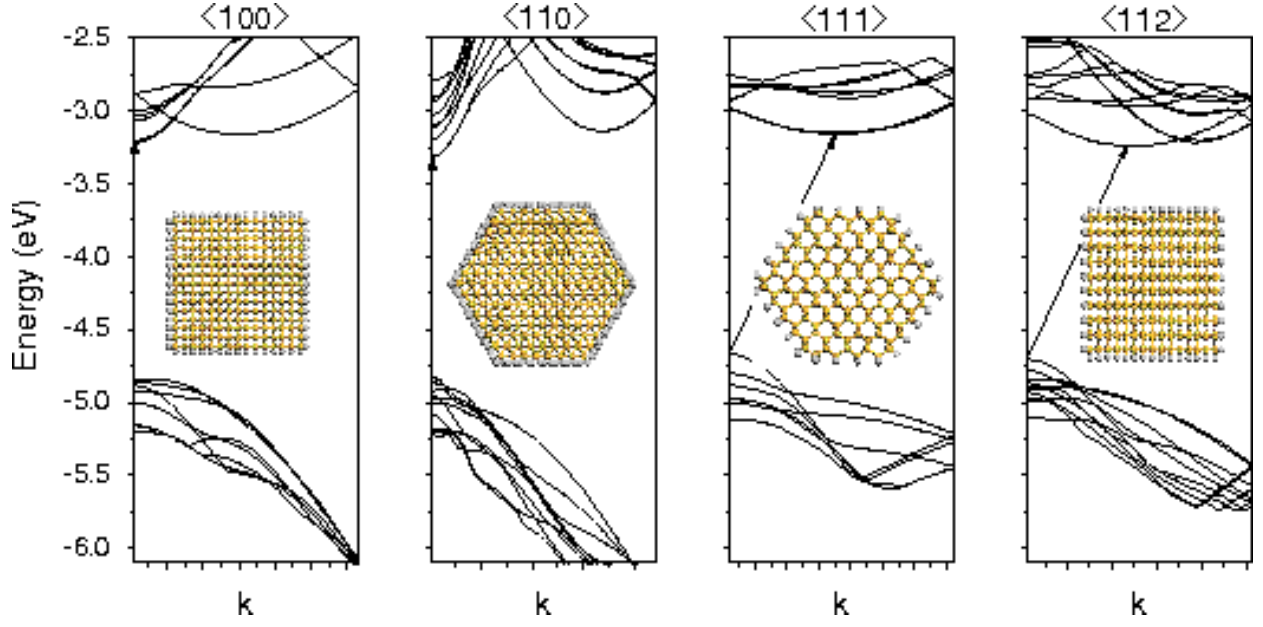


FIG. 9 (Color online) Band structures of $\langle 100 \rangle$ $\langle 110 \rangle$ $\langle 111 \rangle$ and $\langle 112 \rangle$ SiNWs with a diameter of ~ 3.0 nm (cross-sections in the insets). The arrows indicate the fundamental band gap which is direct for $\langle 100 \rangle$ and $\langle 110 \rangle$ SiNWs and indirect for $\langle 111 \rangle$ and $\langle 112 \rangle$ SiNWs. As discussed in the text the band gap of $\langle 111 \rangle$ SiNWs becomes direct when the diameter is reduced below 2 nm. Adapted from Ng *et al.* (2007).

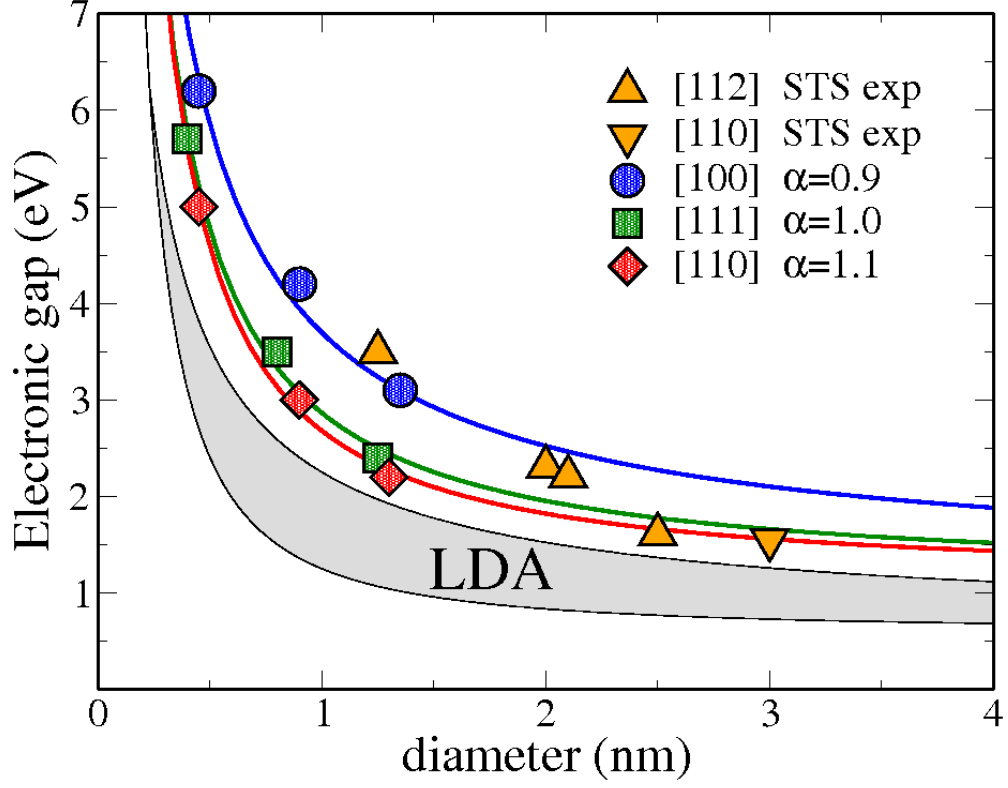


FIG. 10 (Color online) Quasi-particle GW gaps for $\langle 100 \rangle$ (circles), $\langle 111 \rangle$ (squares), and $\langle 110 \rangle$ (diamonds) SiNWs as a function of wire size compared with experimental results (triangles) from scanning tunneling spectroscopy (Ma *et al.*, 2003). The gray region represents the LDA electronic gaps from $\langle 110 \rangle$ (bottom) to $\langle 100 \rangle$ (top) wires. From Bruno *et al.* (2007a).

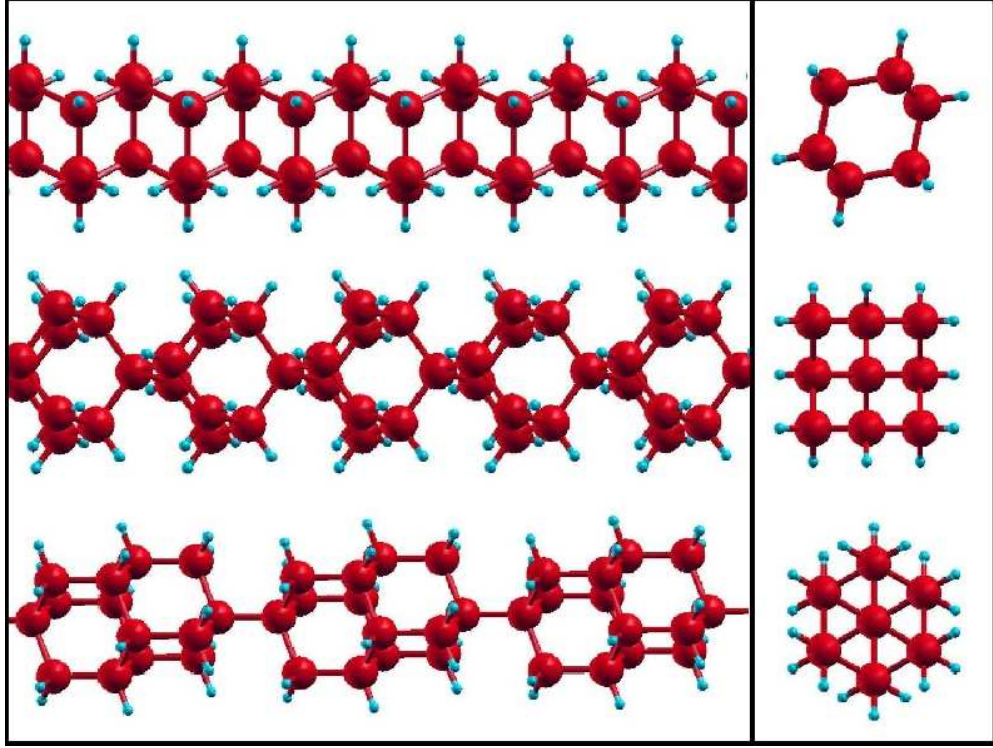


FIG. 11 (Color online) Geometrical structures of 0.4 nm Ge nanowires along the $\langle 110 \rangle$ (top), $\langle 111 \rangle$ (middle), and $\langle 100 \rangle$ (bottom) directions shown from the side (left) and from the top (right). Large spheres represent Ge atoms; small spheres are hydrogen atoms used to saturate the dangling bonds. Adapted from Bruno *et al.* (2005).

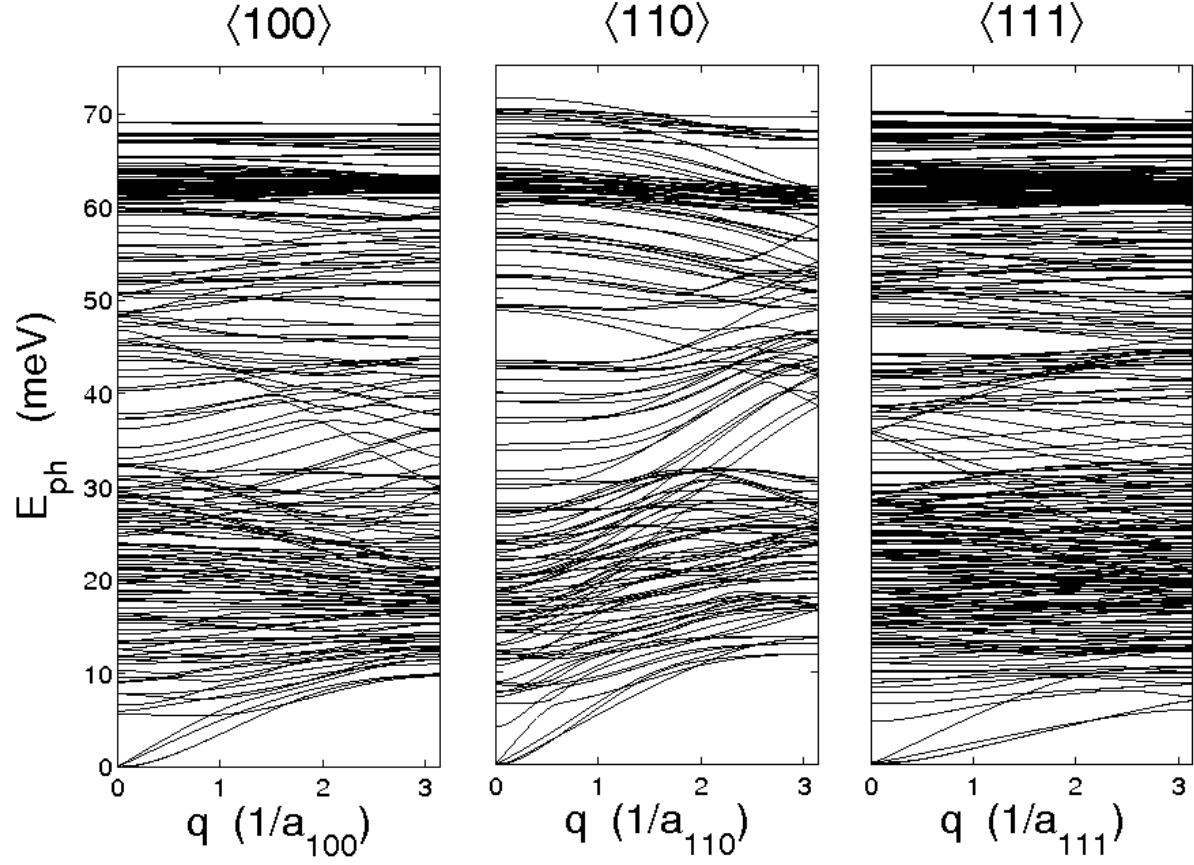


FIG. 12 Phonon band structures calculated within the Tersoff bond-order potential of 2 nm diameter SiNWs grown along the (a) $\langle 100 \rangle$ (b) $\langle 110 \rangle$ and (c) $\langle 111 \rangle$ axis. The phonon wave vectors, q , are all in the respective wire directions and are shown in units of the reciprocal unit cell lengths, with $a_{100} = 5.4$, $a_{110} = 3.8$, and $a_{111} = 9.4$ Å. From Markussen *et al.* (2008a).